Eur. Phys. J. C (2025) 85:94
https://doi.org/10.1140/epjc/s10052-025-13741-w

THE EUROPEAN PHYSICAL JOURNAL C



Regular Article - Theoretical Physics

# Dark coloured scalars impact on single and di-Higgs production at the LHC

**Pedro Gabriel**[1,2,a], **Margarete Mühlleitner**[2,b], **Daniel Neacsu**[3,c], **Rui Santos**[1,4,d]

[1] Centro de Física Teórica e Computacional, Faculdade de Ciências, Universidade de Lisboa, Campo Grande, Edifício C8, 1749-016 Lisbon, Portugal
[2] Institute for Theoretical Physics, Karlsruhe Institute of Technology, Wolfgang-Gaede-Str. 1, 76131 Karlsruhe, Germany
[3] LIP-Laboratório de Instrumentação de Física Experimental de Partículas, Complexo Interdisciplinar (3is), Av. Gama Pinto, n.2, piso 3., 1649-003 Lisbon, Portugal
[4] ISEL-Instituto Superior de Engenharia de Lisboa, Instituto Politécnico de Lisboa, 1959-007 Lisbon, Portugal

Received: 31 July 2024 / Accepted: 20 December 2024


**Abstract** The search for Dark Matter (DM) at colliders is primarily pursued via the detection of missing energy in particular final states. These searches are based on the production and decay processes where final states include DM particles and at least one Standard Model (SM) particle. DM will then reveal itself as missing energy. An alternative form to get a hint of a dark sector is via loop contribution to SM processes. In this case, it is not even relevant if the new particles have their origin in the dark sector of the model. In this work we discuss the impact of an arbitrary number of coloured scalars with $Z_2$-odd parity in single Higgs and double Higgs production at the Large Hadron Collider (LHC), and we show their complementarity. We determine the range of variation of the corrections relative to the SM for an arbitrary number of coloured scalars $n$. We discuss the cases $n = 1$ and $n = 2$ for a specific model in more detail, which includes direct searches at the LHC. We also find that the electroweak observable $T$ parameter imposes significant restrictions on the difference of the heavy coloured scalar masses.

## 1 Introduction

Any extension of the Standard Model (SM) aiming at solving the Dark Matter (DM) puzzle has to include at least one DM candidate. One of the simplest ways to address this problem is to enlarge the scalar sector of the SM by including a dark sector, usually using a discrete symmetry, and a portal coupling that connects the two sectors.[1] Once a minimal model that provides a DM candidate is built, one needs to make sure that it is in agreement with the current measurement of the relic density and with all results from direct and indirect detection together with the constraints imposed by collider experiments. Models with a dark sector can then be further extended to explain other unsolved issues of the SM. Ultimately, any complete extension of the SM has to be in agreement with all available experimental data.

In recent years many models have been proposed to solve other discrepancies between the SM predictions and the experimental results. A particular class of models manages to solve two of these problems simultaneously: the B-physics anomalies, related essentially to the $b \to s\mu^+\mu^-$ transition [1,2] and the muon $g-2$ anomaly [3–7] while providing a sound DM candidate. However, a very recent reinterpretation of the LHCb collaborations completely washed out the discrepancy with the SM prediction in the $b \to s\mu^+\mu^-$ transition [8,9]. Still, this type of models can be made compatible with these new results for $b \to s\mu^+\mu^-$ (compatible with the SM predictions) while still solving the DM and $g-2$ problems.

The existence of this type of models prompted us to study the contribution of the new coloured scalars, that live in the dark sector, to single and di-Higgs production. The models were discussed in great detail in [10,11] and are based on a previous model proposed in [12]. They introduce massive coloured scalar fields which, depending on the charge assignments and $SU(2)$ quantum numbers, can lead to one or several coloured scalars. A discrete $Z_2$ symmetry is imposed

[a] e-mail: ptgabriel@fc.ul.pt
[b] e-mail: margarete.muehlleitner@kit.edu
[c] e-mail: danielstnea@gmail.com
[d] e-mail: rasantos@fc.ul.pt (corresponding author)

[1] We define the dark sector as comprised of the $Z_2$-odd fields, independently of the existence of gauge interactions with the SM bosons.

Published online: 27 January 2025

such that the new fields from the dark sector are odd under $Z_2$ while the SM fields are even under this symmetry. In Ref. [10], three new fields were added to the SM, one $SU(3)_c$ coloured scalar, $\Phi_3$, one colourless scalar, $\Phi_2$, and one vectorlike fermion, $\chi$, with an integer electric charge of 0 or $\pm 1$. The scalars are $SU(2)_L$ singlets and the fermion forms an $SU(2)_L$ doublet. This model was dubbed Model 5. In Ref. [11] a different scenario was studied with the scalars as $SU(2)_L$ doublets and the fermion as an $SU(2)_L$ singlet, and called Model 3.

As the dark sector communicates with the SM via the Higgs potential, the new scalars couple to the Higgs boson. In fact, only two types of interactions are relevant to our discussion: the Higgs couplings to the new coloured scalars and the strong couplings of the coloured scalars with the gluons with origin in the covariant derivative. Therefore the one-loop single Higgs and di-Higgs production only depend on very specific terms in the Higgs potential, the ones that connect the coloured scalars with the SM Higgs doublet. Besides that, the SM Higgs coupling to the fermions (and also the Higgs self-couplings) remain exactly the SM ones[2] - there is no mixing of the Higgs with the other scalars as they have different quantum numbers. The coloured scalars contribute to the gluon fusion single Higgs and di-Higgs production with only one coloured scalar of electric charge $2/3$, $\phi_q^{+2/3}$, in Model 5, while for Model 3 there are two coloured scalars contributing with electric charges $2/3$ and $5/3$, $\phi_q^{+2/3}$ and $\phi_q^{+5/3}$, respectively. We also generalise our results to the case of an arbitrary number of coloured scalars. Note that single Higgs production is a clean probe of the Higgs portal coupling in a scenario where the extension of the SM only includes an arbitrary number of coloured scalars. The di-Higgs cross section can then be used to further confirm the structure suggested by single Higgs production. From now on we will drop the old nomenclature and just refer to the model by the number of coloured scalars.

The LHC has performed numerous searches for DM. The only truly model-independent bound in the case of coloured scalar production and decay (depending only on the mass of the coloured scalar) would be a monojet event, that relies only on the strong gauge coupling. These bounds would be valid in a scenario where the couplings of the coloured scalars to the quarks and vectorlike fermions are negligible or where branching ratios that lead to visible final states are too small to be detected. However, according to [12] the best bounds are obtained in the searches for DM associated with top and bottom quarks [13]. These are more restrictive than a reinterpretation of the searches for squarks at the LHC. They conclude in [12] that the mass of coloured scalars have a rough lower bound of 1 TeV. We will use this bound in our analysis.

We finalise this section by noting that the only new coupling present in the processes to be analysed is the portal coupling. Hence, in the case $n = 1$ all results will depend on only two variables, the portal coupling and the coloured scalar mass. For an arbitrary $n$ we will have $n$ portal couplings and $n$ coloured scalar masses.

The paper is organised as follows. In Sect. 2 we present the single Higgs production mode, and in Sect. 3 the di-Higgs production mode is discussed. In Sect. 4 we compare the contributions of the new physics models to single Higgs and double Higgs production. In Sect. 5 we introduce Model 3 and Model 5 in more detail and discuss probing the parameter space with the electroweak oblique parameters and direct searches at the LHC. Our conclusions are given in Sect. 6.

## 2 Single Higgs production

We consider $n$ independent coloured complex scalars $\phi_q^{i=1,\dots,n}$ transforming in the fundamental representation of $SU(3)_c$. After electroweak symmetry breaking, the potential relevant to this work is given by

$$V = \sum_{i=1}^{n} \Bigg[ \underbrace{(\mu^2_{\phi_q^i} + \frac{v^2}{2}\lambda_{h\phi_q^i})}_{m^2_{\phi_q^i}} |\phi_q^i|^2 + \frac{1}{2}\lambda_{h\phi_q^i} h^2 |\phi_q^i|^2 + v\lambda_{h\phi_q^i} h|\phi_q^i|^2 + \lambda_{\phi_q^i}|\phi_q^i|^4 + \cdots \Bigg] + \cdots \tag{1}$$

where the couplings $\lambda_{h\phi_q^i}$ and $\lambda_{\phi_q^i}$ are real and we have defined the masses of the fields by

$$m^2_{\phi_q^i} = \mu^2_{\phi_q^i} + \frac{v^2}{2}\lambda_{h\phi_q^i}. \tag{2}$$

Note that there are in total $3n$ independent parameters. If we also consider that these $n$ fields form an $SU(2)_L$ multiplet, $\Phi_q = (\phi_q^1 \;\; \phi_q^2 \;\; \dots \;\; \phi_q^n)^{\mathbf{T}}$, this would impose the following constraints: $\mu^2_{\phi_q^i} = \mu^2_{\phi_q^k} \equiv \mu^2_{\Phi_q}$ and $\lambda_{\phi_q^i} = \lambda_{\phi_q^k} \equiv \lambda_{\Phi_q}$.[3] We are now left with only $n+2$ degrees of freedom. This implies that for equal portal couplings $\lambda_{h\phi_q^i}$ the masses $m^2_{\phi_q^i}$ given by Eq. (2) are also equal and vice-versa. For this work we will consider the more general case of $n$ independent fields but

[2] While this statement is only true at tree-level, as loop contributions could in principle change the Higgs to quark couplings, these effects are expected to be small, as the colored scalars are rather heavy, so that their loop contributions are suppressed.

[3] We use uppercase $\Phi$ and lowercase $\phi$ to distinguish between the parameters defined for the multiplet $\Phi$ and the scalars $\phi$.

still assuming that they never have the exact same quantum numbers and thus no mixing.

Single Higgs production via gluon fusion, which is the main production process at the LHC, proceeds at leading order (LO) in the SM via quark loops [14] as shown in Fig. 1a, with the heavier quarks giving the major contribution. In the new models, two new diagrams emerge as shown in Figs. 1b, c.

The amplitude for this process can be cast into the form

$$\mathcal{M}_{\triangle}^{gg\to h} = \frac{g_s^2 m_h^2}{16\pi^2}\left(\sum_Q g_Q^h F_{\triangle}^Q + \sum_{\phi_q^i} g_{\phi_q^i}^h F_{\triangle}^{\phi_q^i}\right) \times A_{1\mu\nu}\,\epsilon_a^\mu \epsilon_b^\nu\,\delta_{ab}, \tag{3}$$

where the indices $a$ and $b$ are associated with the incoming gluons, $A_1^{\mu\nu} = g^{\mu\nu} - p_b^\mu p_a^\nu / p_a \cdot p_b$ and the quark and scalar form factors are given by [15]

$$F_{\triangle}^Q = \tau_Q\left(1 + (1-\tau_Q) f(\tau_Q)\right), \qquad g_Q^h = \frac{1}{v}, \tag{4}$$

$$F_{\triangle}^{\phi_q^i} = -\frac{1}{2}\tau_{\phi_q^i}\left(1 - \tau_{\phi_q^i} f(\tau_{\phi_q^i})\right), \qquad g_{\phi_q^i}^h = \frac{\lambda_{h\phi_q^i} v}{2m_{\phi_q^i}^2}, \tag{5}$$

with $\tau_X = 4m_X^2/m_h^2$ $(X = Q, \phi_q^i)$ and $f(\tau)$ defined as

$$f(\tau) = \begin{cases} \arcsin(\frac{1}{\sqrt{\tau}})^2 & \tau \geq 1 \\ -\frac{1}{4}\left[\log(\frac{1+\sqrt{1-\tau}}{1-\sqrt{1-\tau}}) - i\pi\right]^2 & \tau < 1 \end{cases}. \tag{6}$$

In the limit of large masses the form factors approach a constant value,

$$\lim_{m_Q^2\to\infty} F_{\triangle}^Q = \frac{2}{3} \tag{7}$$

$$\lim_{m_{\phi_q^i}^2\to\infty} F_{\triangle}^{\phi_q^i} = \frac{1}{6} \tag{8}$$

and therefore the large mass behaviour is determined solely by the coupling pre-factors $g_X^h$. Consequently, for large masses, the scalar loop contribution to the amplitude is suppressed by a factor of $1/m_{\phi_q^i}^2$. Because the quark Yukawa couplings are proportional to their masses, the quark loop contribution approaches a constant value for large masses. Thus, although this process can be used to determine how many heavy quarks are present in the model the same is not true for the coloured scalars. In Fig. 2 we present $f(\tau)$ as a function of $\tau$ in the left plot and the quark and scalar form factors as a function of $\tau$ in the right plot, which nicely shows that the two form factors approach constant values in the large mass limit.

### 2.1 The LHC production cross section

The calculation of the gluon fusion production cross section is performed at LO by implementing the new form factors for the coloured scalars (Eq. (5)) in the program HIGLU [16] which can be used to calculate the single Higgs production cross section at the LHC in the SM and in the Minimal Supersymmetric extension of the SM (MSSM). In the SM the $gg$ initiated production is much larger than its quark counterpart making the latter negligible in SM-like models, such as the ones discussed in this work. We can therefore write the hadronic cross section as

$$\sigma(pp\to h) = \sigma_0^h \tau_h \frac{\mathrm{d}\mathcal{L}^{gg}}{\mathrm{d}\tau_h}, \qquad \sigma_0^h = \frac{\pi}{16 m_h^4}\left|\mathcal{M}_{\triangle}^{gg\to h}\right|^2, \tag{9}$$

where $\frac{\mathrm{d}\mathcal{L}^{gg}}{\mathrm{d}\tau_h}$ is the gluon luminosity and $\tau_h = m_h^2/s$, with $s$ denoting the total hadronic c.m. energy squared. In order to reduce the impact of the important higher-order (HO) effects we calculate the relative deviation of the new physics (NP) cross section in our model from the SM cross section, defined as

$$\delta_h = \frac{\sigma_{NP} - \sigma_{SM}}{\sigma_{SM}}. \tag{10}$$

We hence assume that the relative HO corrections to the new physics cross section in our model do not deviate significantly from those of the SM case, for the QCD corrections[4,5] while for the EW corrections[6] this is not necessarily the case. For the former, large differences in the NP and SM QCD corrections are expected to occur at thresholds of the virtual particles. For this work we consider only coloured scalar masses above 1 TeV avoiding these regions. As for the EW corrections, these have shown to be small when compared to the QCD corrections in the SM, of the order of a few percent [65]. Combined with the fact that we calculate relative deviations, the impact of the EW corrections due to new colored scalars should be subleading. Using Eqs. (3–5) and Eq. (9),

[4] In the SM, the gluon fusion cross section is known at next-to-leading order (NLO) QCD including the full mass dependences [17–24]. Within the heavy top-quark limit the next-to-next-to-leading order (NNLO) [25–30] and next-to-next-to-next-to leading order ($N^3LO$) [31–38,38–41] QCD corrections have been calculated. An explicit large top-mass expansion has estimated the missing quark-mass effects beyond NLO to be less than 1% [42–45]. Quark mass effects in two-loop Higgs amplitudes have been given in [46]. The exact mass dependence of the Higgs-gluon form factor at three loops in QCD has been provided in [47,48].

[5] For coloured scalars the corrections for different models can be found in [22,23,49–59].

[6] The NLO EW corrections have been calculated in [60–66] and the mixed QCD-EW corrections in [67].

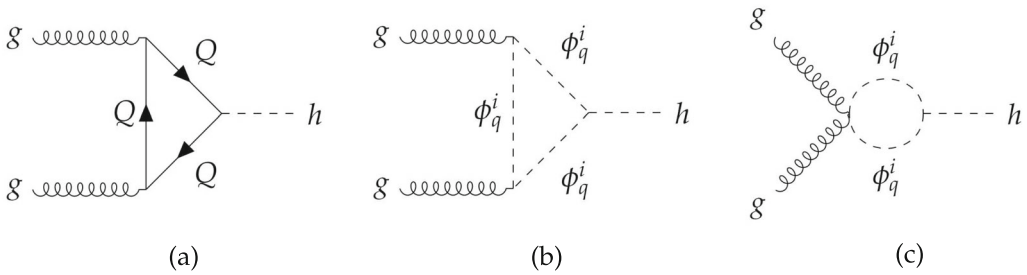


**Fig. 1** Generic single Higgs production diagrams. **a** SM quark loop; **b**, **c** coloured scalar loop

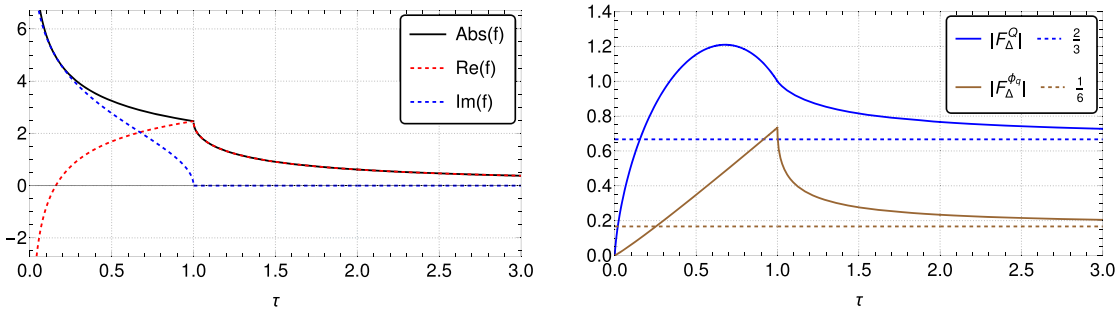


**Fig. 2** Left: $f(\tau)$ as a function of $\tau$; right: quark and scalar form factors as a function of $\tau$

we can write $\delta_h$ as

$$\delta_h = \frac{\left|\sum_Q F_\triangle^Q + v\sum_{\phi_q^i} g^h_{\phi_q^i} F_\triangle^{\phi_q^i}\right|^2 - \left|\sum_Q F_\triangle^Q\right|^2}{\left|\sum_Q F_\triangle^Q\right|^2}$$
$$= 2v\sum_{\phi_q^i} g^h_{\phi_q^i}\,\mathrm{Re}\left[\frac{F_\triangle^{\phi_q^i}}{\sum_Q F_\triangle^Q}\right] + v^2\frac{\left|\sum_{\phi_q^i} g^h_{\phi_q^i} F_\triangle^{\phi_q^i}\right|^2}{\left|\sum_Q F_\triangle^Q\right|^2}. \tag{11}$$

For the following numerical analysis we include the bottom, charm and top quark loops in single Higgs production, while in double Higgs production only top and bottom quark loops are taken into account.[7] We use the following input values for the Higgs, top, bottom and charm quark masses, respectively:

$$m_h = 125\ \text{GeV}, \quad m_t = 172.5\ \text{GeV},$$
$$m_b = 4.75\ \text{GeV}, \quad m_c = 1.43\ \text{GeV}. \tag{12}$$

We use the LO pdfs NNPDF40_lo_as_01180 [68,69] and the LO strong coupling constant

$$\alpha_s(m_Z) = 0.118 \tag{13}$$

for which the running of $\alpha_s$ is included at LO.[8] The cross sections are calculated for a c.m. energy of $\sqrt{s} = 14$ TeV. Note that the dependence on $\sqrt{s}$ cancels out in $\delta_h$ at LO.

### 2.2 Model with one scalar versus a model with two scalars

Let us start by considering the scenarios $n = 1$ (just one coloured scalar) and $n = 2$ (two coloured scalars). As already discussed, all scalar masses will be taken to be above 1 TeV. In the case $n = 1$ and considering here, for the sake of the discussion, only the top quark contribution (the bottom contribution only ranges at the percent level), the following simplified form for $\delta_h$ is obtained

$$\delta_h = \lambda_{h\phi_q^1}\frac{v^2}{m^2_{\phi_q^1}}\left(\frac{F_\triangle^{\phi_q^1}}{F_\triangle^Q}\right) + \lambda^2_{h\phi_q^1}\frac{v^4}{4m^4_{\phi_q^1}}\left(\frac{F_\triangle^{\phi_q^1}}{F_\triangle^Q}\right)^2. \tag{14}$$

Any extension with more than one coloured scalar will have one more effective Higgs-scalar coupling $\lambda_{h\phi_q^i}$ and one more scalar mass $m_{\phi_q^i}$ for each new scalar added to the model. Thus, in order to simplify the presentation of the results, we impose the constraint of equal coloured scalar masses for any extension with more than one coloured scalar. As we will show later, for masses above 5 TeV the cross sections will be very small unless the number of scalars becomes very large. So the interesting range for the mass is indeed very small.

[7] This choice is based on the quarks the original HIGLU and HPAIR codes include, however we have checked that excluding the charm loops in single Higgs production for consistency would produce a negligible difference.

[8] The scale used in the calculation of $\alpha_s$ is chosen to be equal to $M_h/2$ for HIGLU and $M_{hh}/2$ for HPAIR.

Note that in the plots presented later we will always include the bottom, charm and top contributions.

The quartic coupling $\lambda_{h\phi_q^i}$ that enters the calculation of the cross section is an effective coupling in the following sense: in the case $n = 1$ it is just the portal coupling between the Higgs and the singlet coloured scalar; for $n = 2$, the two effective couplings are the sum of combinations of three portal couplings (in the case of an $SU(2)$ representation). In more detail, for $n = 1$ the coloured scalar is an $SU(2)$ singlet and the portal coupling with the Higgs doublet can be written as

$$V_{\text{portal}}^{n=1} = \lambda_{H\Phi_q}|H|^2|\Phi_q|^2, \tag{15}$$

and the effective coupling takes the form

$$\lambda_{h\phi_q^1} = \lambda_{H\Phi_q}\,. \tag{16}$$

In the scenario $n = 2$ the coloured scalar is an $SU(2)$ doublet and the portal couplings are now

$$\begin{aligned} V_{\text{portal}}^{n=2} = {} & \lambda_{H\Phi_q}|H|^2|\Phi_q|^2 + \lambda'_{H\Phi_q}|H^\dagger\Phi_q|^2 \\ & + \Lambda_{H\Phi_q}|H^\dagger i\sigma_2\Phi_q|^2, \end{aligned} \tag{17}$$

which results in two effective couplings,

$$\begin{aligned} \lambda_{h\phi_q^1} &= \lambda_{H\Phi_q} + \lambda'_{H\Phi_q} \\ \lambda_{h\phi_q^2} &= \lambda_{H\Phi_q} + \Lambda_{H\Phi_q}. \end{aligned} \tag{18}$$

We have also checked that the same applies to the triplet representation of $SU(2)$ [70]. However, one should stress that what is relevant here is that we will discuss any type of model with an arbitrary number of scalars, each with an effective portal coupling and a given mass. The results can then be translated to any specific model of this kind.

Since all form factors are positive and strictly decreasing for $m_{\phi_q^i} > 1$ TeV, the highest contributions to the cross sections will be achieved when these form factors are at their highest value corresponding to the lowest mass for all the scalars. Under the equal masses constraint ($m_{\phi_q^i} = m_{\phi_q^j} \equiv m_{\phi_q} \Rightarrow F_\triangle^{\phi_q^i} = F_\triangle^{\phi_q^j} \equiv F_\triangle^{\phi_q}$) we can write

$$\begin{aligned} \delta_h = {} & \left(\sum_i \lambda_{h\phi_q^i}\right)\frac{v^2}{m_{\phi_q}^2}\left(\frac{F_\triangle^{\phi_q}}{F_\triangle^{Q}}\right) \\ & + \left(\sum_i \lambda_{h\phi_q^i}\right)^2 \frac{v^4}{4m_{\phi_q}^4}\left(\frac{F_\triangle^{\phi_q}}{F_\triangle^{Q}}\right)^2. \end{aligned} \tag{19}$$

With all masses equal, $\delta_h$ is not sensitive to individual couplings but only to their total sum, $\sum_i \lambda_{h\phi_q^i}$. Further, taking all couplings equal, $\lambda_{h\phi_q^i} = \lambda_{h\phi_q^j} \equiv \lambda_{h\phi_q}$, we still cover the full range of possible values for $\delta_h$ because for any particular choice of couplings $\{\lambda_{h\phi_q^1}, \ldots, \lambda_{h\phi_q^n}\}$ there is always a single coupling $\lambda_{h\phi_q}$ such that $\sum_i \lambda_{h\phi_q^i} = n\lambda_{h\phi_q}$ which will give equivalent results for $\delta_h$. With this approximation the coupling $\lambda_{h\phi_q}$ will just be rescaled by a factor $n$ when going from the case $n = 1$ to arbitrary $n$.

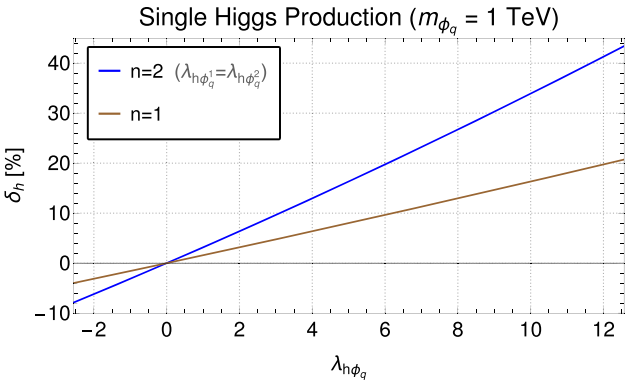


**Fig. 3** $\delta_h$ as a function of the effective portal coupling $\lambda_{h\phi_q}$ for a mass of $m_{\phi_q} = 1$ TeV and for $n = 1$ and $n = 2$

Before presenting the results we will discuss the allowed values for the couplings. As the upper bound we will consider the perturbativity bound of $4\pi$. For the lower bound, one of the conditions for the potential (Eq. (1)), to be bounded from below, following the same procedure as in [71], gives rise to the following constraint at LO

$$\lambda_{h\phi_q^i} \geq -\frac{m_h}{v}\sqrt{2\lambda_{\phi_q^i}}, \tag{20}$$

where $m_h$ is the SM Higgs boson mass and $\lambda_{\phi_q^i}$ is the $\phi_q^i$ quartic self coupling parameter that must be positive, $\lambda_{\phi_q^i} \geq 0$, and obey the perturbativity bound of $\lambda_{\phi_q^i} \leq 4\pi$. Therefore we will vary the relevant parameters $\lambda_{h\phi_q^i}$ between the lower value given by Eq. (20) and the upper value $4\pi$.

In Fig. 3 we present the results for $\delta_h$ as a function of the effective portal coupling $\lambda_{h\phi_q}$ for a mass of $m_{\phi_q} = 1$ TeV and for $n = 1$ and $n = 2$. The single Higgs cross section was calculated with `HIGLU` for a c.m. energy of 14 TeV resulting in a SM LO cross section of $\sigma_{SM}^h = 15.76$ pb for the above given input values. It is evident that $\delta_h$ varies linearly with the effective coupling $\lambda_{h\phi_q}$, which means that, in this range, the interference term between the SM and NP form factors is dominant. The large scalar masses we are working with and the fact that the interference term is proportional to only $1/m_{\phi_q}^2$ while the purely NP contributions are suppressed by a factor of $1/m_{\phi_q}^4$ (cf. Eq. (14)), are the reasons behind this behaviour.

In Fig. 4 we show the results for $\delta_h$ as a function of the coloured scalar mass for the minimum value of the coupling (left) and the maximum value of the coupling (right) and for $n = 1$ and $n = 2$. Since, as argued above, the interference term is dominant, $\delta_h$ behaves approximately as $1/m_{\phi_q}^2$ for fixed $\lambda_{h\phi_q}$. For the allowed range of variation the maximum

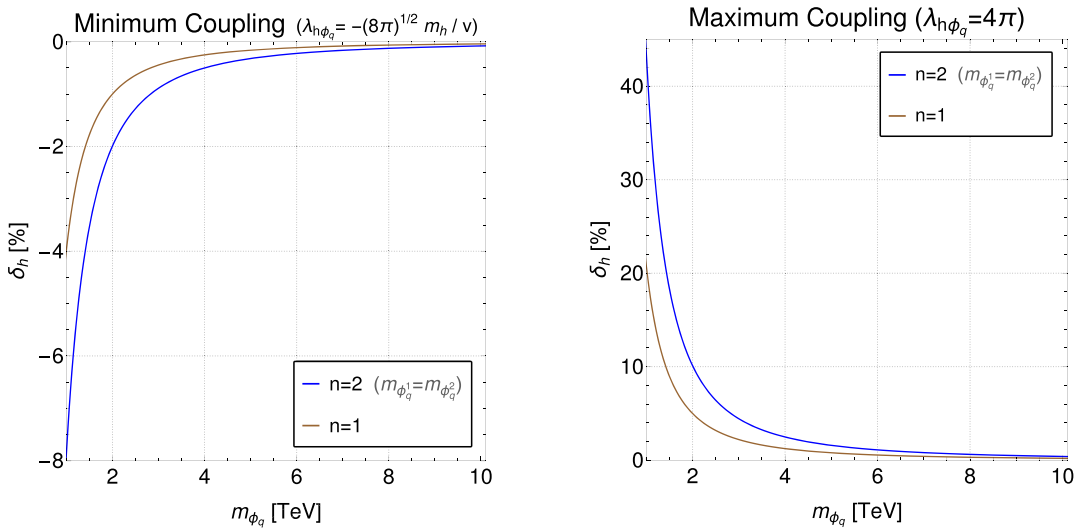


**Fig. 4** $\delta_h$ as a function of the coloured scalar mass for the minimum value of the coupling (left) and the maximum value of the coupling (right) and for $n = 1$ and $n = 2$

value of variation relative to the SM is between about -10% and +40%.

The NP term only becomes comparable to the interference term in the limit

$$\lambda_{h\phi_q} = \frac{4m_{\phi_q}^2}{v^2}\frac{F_\triangle^Q}{F_\triangle^{\phi_q}} \xrightarrow[m_{\phi q}\to\infty]{m_Q\to\infty} \frac{16m_{\phi_q}^2}{v^2}, \tag{21}$$

which means that for a mass of $m_{\phi_q} = 1$ TeV $\lambda_{h\phi_q} \approx 260$ for $n = 1$. As more scalars are added the picture can change. As the interference term scales with $n$ and the NP term scales as $n^2$, for a number of scalars above 20 and all masses equal to 1 TeV the NP term starts to dominate.

### 2.3 Models with $n$ coloured scalars

In the previous section we have set all masses to be equal. Relaxing this condition forces us to return to the more general expression given in Eq. (11). However, we can follow a different approach in order to simplify the final expression by taking advantage of the large scalar masses and using the limit for $F_\triangle^{\phi_q^i}$ given in Eq. (8). For scalar masses above 1 TeV the error in $F_\triangle^{\phi_q^i}$ by using this limit is only about 0.2%. With this approximation $\delta_h$ can be written as

$$\delta_h = \frac{1}{\left|\sum_Q F_\triangle^Q\right|}\frac{v^2}{6}\sum_i \frac{\lambda_{h\phi_q^i}}{m_{\phi_q^i}^2} + \frac{1}{\left|\sum_Q F_\triangle^Q\right|^2}\frac{v^4}{144}\left(\sum_i \frac{\lambda_{h\phi_q^i}}{m_{\phi_q^i}^2}\right)^2, \tag{22}$$

where we have $\left|\sum_Q F_\triangle^Q\right| \approx 0.641$ when including the top, bottom and charm quarks. Including only the top quark and the limit in Eq. (7) would imply an error in $\left|\sum_Q F_\triangle^Q\right|$ of around 4%. This approximation has the advantage of allowing us to write the results as a function of the ratio $x_i = \lambda_{h\phi_q^i}/m_{\phi_q^i}^2$ where the index $i$ represents each scalar.[9] It is now clear that we can show $\delta_h$ as a function of the sum $(\sum_i x_i)$. As previously discussed, as long as we span all possible values for this sum we will also have fully explored all values that $\delta_h$ can take. In order to do this let us first note that the minimum and maximum of $(\sum_i x_i)$ are achieved when all $x_i$ are at their minimum and maximum values, respectively. Hence, to generate all values for the sum and consequently for $\delta_h$, we can make the simple choice of $x_i = x_j$ with the limits of $\min(x_i) = \min\left(\lambda_{h\phi_q^i}/m_{\phi_q^i}^2\right) = -(8\pi)^{1/2} m_h/v\ \text{TeV}^{-2}$ and $\max(x_i) = \max\left(\lambda_{h\phi_q^i}/m_{\phi_q^i}^2\right) = 4\pi\ \text{TeV}^{-2}$ where we have considered $\min(m_{\phi_q^i}) = 1$ TeV.

In Fig. 5 we show $\delta_h$ as a function of $\sum_i x_i$. The minimum and maximum limits for a model with $n$ scalars are indicated by the coloured zones, where a minimum mass of 1 TeV is considered and the couplings are varied between their minimum and maximum allowed values.

[9] This approximation is not strictly necessary. In the general case the ratio would be $x_i = \lambda_{h\phi_q^i}\frac{F_\triangle^{\phi_q^i}}{m_{\phi_q^i}^2}$. All conclusions in this section are only dependent on the fact that $x_i$ decreases with mass, a behaviour present whether we use the approximation or not since $F_\triangle^{\phi_q^i}$ approaches a constant value for large masses and $\lambda_{h\phi_q^i}$ takes a constant value between its boundaries.

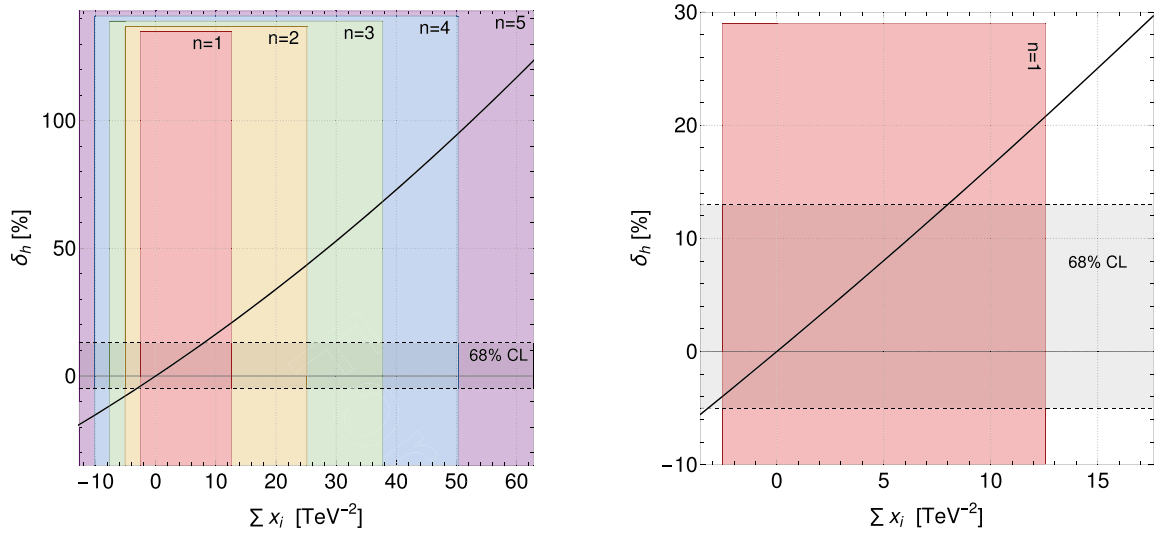


**Fig. 5** $\delta_h$ as a function of $\sum_i x_i$. The minimum and maximum limits for a model with $n$ scalars are indicated by the coloured zones, where a minimum mass of $m_{\phi_q^i} = 1$ TeV is considered and the couplings are varied between the lower bound of $-(8\pi)^{1/2} m_h/v$ and the perturbativity upper bound of $4\pi$. In the left plot the horizontal lines are taken from the ATLAS combination [72] and show the $1\sigma$ results for Higgs production via gluon fusion. In the right plot we present just the case $n = 1$ for a better understanding of the bounds on $\sum_i x_i$ for $n = 1$

The horizontal lines represent the relative experimental uncertainty of the experimental results for Higgs production via gluon fusion at $1\sigma$ with Higgs SM branching ratios assumed.[10] In the left plot the lines are taken from the ATLAS combination [72] at 13 TeV and 80 fb$^{-1}$, leading to $\delta_h \in [-5, 13]$ %. In the right plot we present just the case $n = 1$ for a better understanding of the bounds on $\sum_i x_i$ for $n = 1$. Considering $n = 1$ we can see that $-3.2 < \sum_i x_i < 8$ approximately. This in turn means that for a mass of 1 TeV the coupling is also constrained to be $-3.2 < \lambda_{h\phi_q^1} < 8$. Therefore the bounds are not very strong at the moment but are already better than the perturbative limit for the upper bound. Still, as the mass grows the bound on the coupling gets weaker. For $n > 1$ if the couplings are all of the same order, the constraints will be stronger if again the masses are all of the order 1 TeV. But there is always the possibility of having all couplings very small except one, recovering the $n = 1$ constraints for the larger coupling. Furthermore, if the couplings have different signs we end up with a larger freedom than for the case $n = 1$. These scenarios will have to be studied for the specific model in question using every other information on the model.

In Fig. 6 we show the allowed values of $\delta_h$ (left) and $\sum_i x_i$ (right) at $1\sigma$ and $2\sigma$ using the present experimental limits from ATLAS [72], CMS [73], and the projections for the future HL-LHC [74]. The projections for the HL-LHC show that we will attain a result of the order $\delta_h \in [-1.6, 1.6]$ %. Note that this assumes that the overall uncertainty scales with the luminosity as $1/\sqrt{L}$ and we take the SM as the central value.

[10] The branching ratios are dependent on the model and thus, for this work, we consider only the SM branching ratios.

### 2.4 Higgs to gluons decay

In the SM, the partial width of the $H \to gg$ decay is calculated to be around $\Gamma^{gg}_{SM} = 0.335$ MeV [75], representing a branching ratio of about 8.2 %. On the other hand, the branching ratio for the neutral electroweak bosons, $\gamma\gamma$ and $\gamma Z$, are significantly smaller with a value of around 0.2 % each. The $ZZ$ decay is slightly larger with 2.6 % but still smaller then the gluons. The coloured scalars will contribute to these decay modes. For the electroweak branching ratios, which are already very small in the SM, the contributions will be suppressed by $\alpha^2_{EW}/\alpha^2_s$ when compared to the gluons decay. Additionally, other NP electrically charged fields in the models would need to be taken into account. For this reason, for this work we only consider the gluons decay.

At LO the decay $H \to gg$ has the same diagrams (Fig. 1) as the gluon fusion production (Eq. 9) and the two only differ by an overall factor:

$$\Gamma^{gg}_{LO} = \frac{1}{2\pi m_h} \left| \mathcal{M}^{h\to gg}_{\triangle} \right|^2 ,$$
$$\Gamma^{gg}_{LO} = \frac{8 m_h^3}{\pi^2} \sigma^h_0 . \tag{23}$$

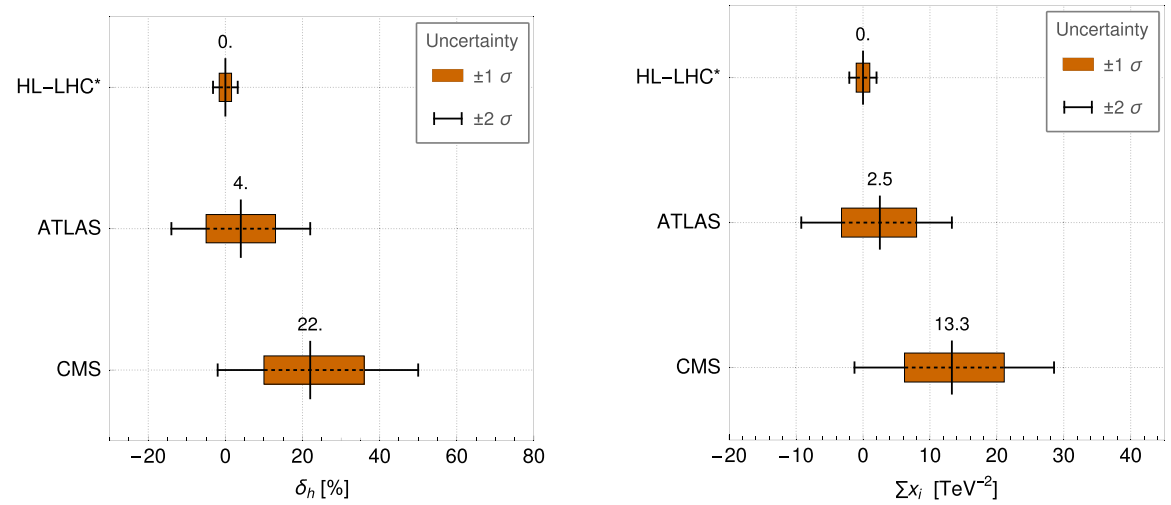


**Fig. 6** Allowed values of $\delta_h$ (left) and $\sum_i x_i$ (right) at $1\sigma$ and $2\sigma$ using the present experimental limits from ATLAS [72], CMS [73], and the projections for the future HL-LHC [74]

Following the approach in [72] (Sec 7.1) we define the coupling-strength modifier, $\kappa_{gg}$, as

$$\kappa_{gg}^2 = \frac{\Gamma_{NP}^{gg}}{\Gamma_{SM}^{gg}}. \tag{24}$$

We can also again define the relative difference, $\delta_{gg}$, and relate the two variables by

$$\delta_{gg} = \frac{\Gamma_{NP}^{gg} - \Gamma_{SM}^{gg}}{\Gamma_{SM}^{gg}}, \quad \kappa_{gg}^2 = 1 + \delta_{gg}. \tag{25}$$

From Eq. 23 we conclude that this relative difference is the same as for Higgs production (Eq. 10) and we can take $\delta_{gg} = \delta_h$. Then the results from the previous sections can be applied in the same way as in Fig. 5.

In Fig. 7 we show the coupling-strength modifier, $\kappa_{gg}$, as a function of $\sum_i x_i$. The minimum and maximum limits for a model with $n$ scalars are indicated by the coloured zones, where a minimum mass of 1 TeV is considered and the couplings are varied between their minimum and maximum allowed values. The horizontal lines represent the constraints to the coupling-strength modifier, $\kappa_{gg}$. The full black lines are calculated from experimental data at ATLAS [72] Sec. 7.3) leading to $\kappa_{gg}^{ATLAS} = 1.03^{+0.07}_{-0.06}$. This corresponds to a cut on the parameter space of around $-3.8 < \sum_i x_i < 12.7$. On the other hand, the horizontal dashed lines are the expected $1\sigma$ uncertainties at the HL-LHC given in [74] (Sec. 2.7 - Fig. 30) with a value of $\Delta\kappa_{gg}^{HL-LHC} = \pm 0.025$. This in turn corresponds to a cut of $-3.2 < \sum_i x_i < 3.2$. With the coupling-strength modifier framework we have tested the constraints from the loop induced contributions to the partial width of the $H \to gg$ decay due to the coloured scalars. The limits resulting from the decay are thus of the same order as the ones for the Higgs production process.

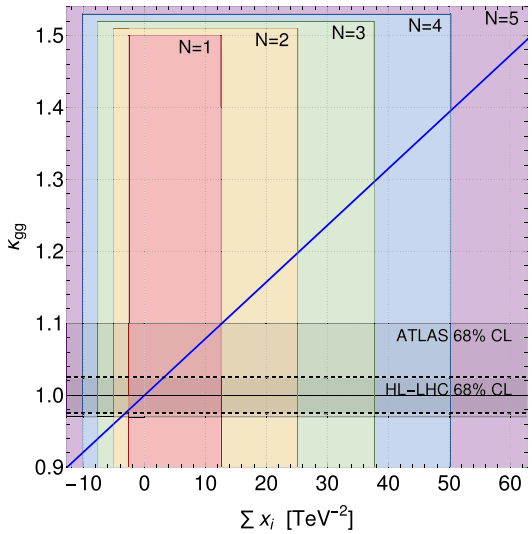


**Fig. 7** The blue line represents the coupling-strength modifier $\kappa_{gg}$ as a function of $\sum_i x_i$. The minimum and maximum limits for a model with $n$ scalars are indicated by the coloured zones, where a minimum mass of $m_{\phi_q^i} = 1$ TeV is considered and the couplings are varied between the lower bound of $-(8\pi)^{1/2} m_h/v$ and the perturbativity upper bound of $4\pi$. The black horizontal lines represent the $1\sigma$ constraints taken from [72] while the dashed horizontal lines represent the expected uncertainties at the HL-LHC taken from [74]

## 3 Double Higgs production

Similar to the single Higgs case, the production of a pair of Higgs bosons is dominated by the gluon fusion process, which at LO is given by a triangle and a box diagram with heavy quarks running in the loop [76]. The new coloured scalars will contribute to di-Higgs production by similar loop diagrams. Due to the new 2 gluon-2 coloured scalars and 2

Higgs-2 coloured scalars couplings, however, there are now additional topologies that contribute to the process.

### 3.1 The leading-order amplitude

The complete set of diagrams is given by the ones involving the trilinear Higgs self-coupling, shown in Fig. 8, and diagrams that do not depend on it, depicted in Fig. 9. The new topologies arising in our model are given in Fig. 8b, c and in Fig. 9b–e. As in the SM, we have triangle and box topologies and now additionally also a self-energy-like topology.

The LO amplitude can be decomposed into two different tensor structures, which correspond to total gluon spin 0 and 2, respectively, along the collision axis. They are given by [77]

$$A_1^{\mu\nu} = g^{\mu\nu} - \frac{p_b^\mu p_a^\nu}{(p_a p_b)} \tag{26}$$

$$A_2^{\mu\nu} = g^{\mu\nu} + \frac{1}{p_T^2 (p_a p_b)} \times \left[ \left( p_c^2 \right) p_b^\mu p_a^\nu - 2\,(p_b p_c)\, p_c^\mu p_a^\nu - 2\,(p_a p_c) \times p_b^\mu p_c^\nu + 2\,(p_a p_b)\, p_c^\mu p_c^\nu \right] \tag{27}$$

with

$$A_1 \cdot A_1 = A_2 \cdot A_2 = 2, \quad A_1 \cdot A_2 = 0 \tag{28}$$

and

$$p_T^2 = 2\frac{(p_a p_c)\,(p_b p_c)}{(p_a p_b)} - p_c^2, \tag{29}$$

where $p_{a,b}$ denote the four-momenta of the two incoming gluons, and $p_{c,d}$ those of the outgoing Higgs bosons. The LO amplitude given by the diagrams in Fig. 8, which contain the trilinear Higgs self-coupling, can be cast in the form

$$\mathcal{M}_{hhh}^{gg\to hh} = \frac{g_s^2 s}{16\pi^2}\, C_\triangle \times \left( \sum_Q g_Q^h F_\triangle^Q + \sum_{\phi_q^i} g_{\phi_q^i}^h F_\triangle^{\phi_q^i} \right) A_{1\mu\nu} \epsilon_a^\mu \epsilon_b^\nu\, \delta_{ab} \tag{30}$$

where $\epsilon_{a,b}^{\mu/\nu}$ represent the gluon polarisation vectors, $g_s$ denotes the strong coupling constant and the constant

$$C_\triangle = \frac{3m_h^2/v}{s - m_h^2} \tag{31}$$

has the tree-level trilinear Higgs self-coupling in the numerator. The first term in Eq. (30) corresponds to the first diagram and the second one to the last two diagrams.[11] The form factors $F_\triangle^{Q/\phi_q^i}$ and the couplings $g^h_{Q/\phi_q^i}$ are given in Eqs (4) and (5). The amplitude independent of the Higgs self-coupling can be written as

$$\mathcal{M}_{\text{no } hhh}^{gg\to hh} = \frac{g_s^2 s}{16\pi^2}\, C_\square \times \Bigg[ \sum_Q \left( (g_Q^h)^2 F_\square^Q A_{1\mu\nu} + (g_Q^h)^2 G_\square^Q A_{2\mu\nu} \right) + \sum_{\phi_q^i} \left( \left( (g^h_{\phi_q^i})^2 F_{\square_1}^{\phi_q^i} + g^{hh}_{\phi_q^i} F_{\square_2}^{\phi_q^i} \right) A_{1\mu\nu} + (g^h_{\phi_q^i})^2 G_{\square_1}^{\phi_q^i} A_{2\mu\nu} \right) \Bigg] \epsilon_a^\mu \epsilon_b^\nu\, \delta_{ab}\,, \tag{32}$$

where $C_\square = 1$, the prefactors $g^h_{Q/\phi_q^i}$ are given in Eqs. (4) and (5) and

$$g^{hh}_{\phi_q^i} = \frac{\lambda_{h\phi_q^i}}{2m^2_{\phi_q^i}}. \tag{33}$$

The quark form factors $F_\square^Q$ and $G_\square^Q$ corresponding to Fig. 9 (a), which have been calculated in the literature before (cf. e.g. [77]), are deferred to the Appendix B, while the new form factors are given here. The form factor $F_{\square_1}^{\phi_q^i}$ sums the contributions of the diagrams Fig. 9b, c proportional to $A_1^{\mu\nu}$, $F_{\square_2}^{\phi_q^i}$ stems from the sum of the contributions of Fig. 9d, e, and $G_{\square_1}^{\phi_q^i}$ is the sum of the contributions of Fig. 9b, c proportional to $A_2^{\mu\nu}$. They read explicitly[12]

$$G_{\square_1}^{\phi_q} = \frac{4m_{\phi_q}^4}{s}\left(\frac{1}{tu - m_h^4}\right) \times \Big( s(t+u) C_{ab}^{m^2_{\phi_q}} + (2t)(t - m_h^2) C_{ac}^{m^2_{\phi_q}} + (2u)(u - m_h^2) C_{bc}^{m^2_{\phi_q}} - (t^2 + u^2 - 2m_h^4) C_{cd}^{m^2_{\phi_q}} - (st^2 + 2m^2_{\phi_q}(tu - m_h^4)) D_{bac}^{m^2_{\phi_q}} - (su^2 + 2m^2_{\phi_q}(tu - m_h^4)) D_{abc}^{m^2_{\phi_q}} - (2m^2_{\phi_q}(tu - m_h^4)) D_{acb}^{m^2_{\phi_q}} \Big) \tag{34}$$

$$F_{\square_1}^{\phi_q} = \frac{4m_{\phi_q}^4}{s}\left( \frac{2}{s}(t - m_h^2) C_{ac}^{m^2_{\phi_q}} + \frac{2}{s}(u - m_h^2) C_{bc}^{m^2_{\phi_q}} - (2m^2_{\phi_q})(D_{abc}^{m^2_{\phi_q}} + D_{bac}^{m^2_{\phi_q}}) \right)$$

[11] In accordance with the FeynArts [78,79] notation, we call triangle diagrams loops with three legs attached and box diagrams loops with four legs attached.

[12] See also e.g. [80,81]. In the former paper, the authors focused on the impact of light coloured scalars on di-Higgs production while in the latter the effect of light coloured scalar leptoquarks was analysed.

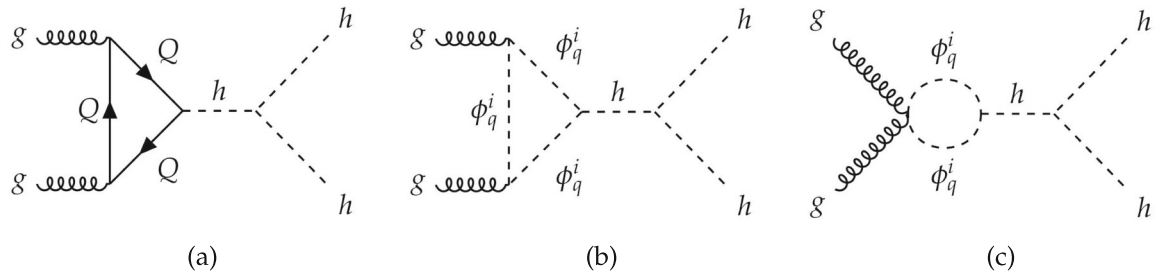


**Fig. 8** Generic diagrams contributing to double Higgs production involving the trilinear Higgs self-coupling: **a** SM quark loop; **b**, **c** coloured scalar loop

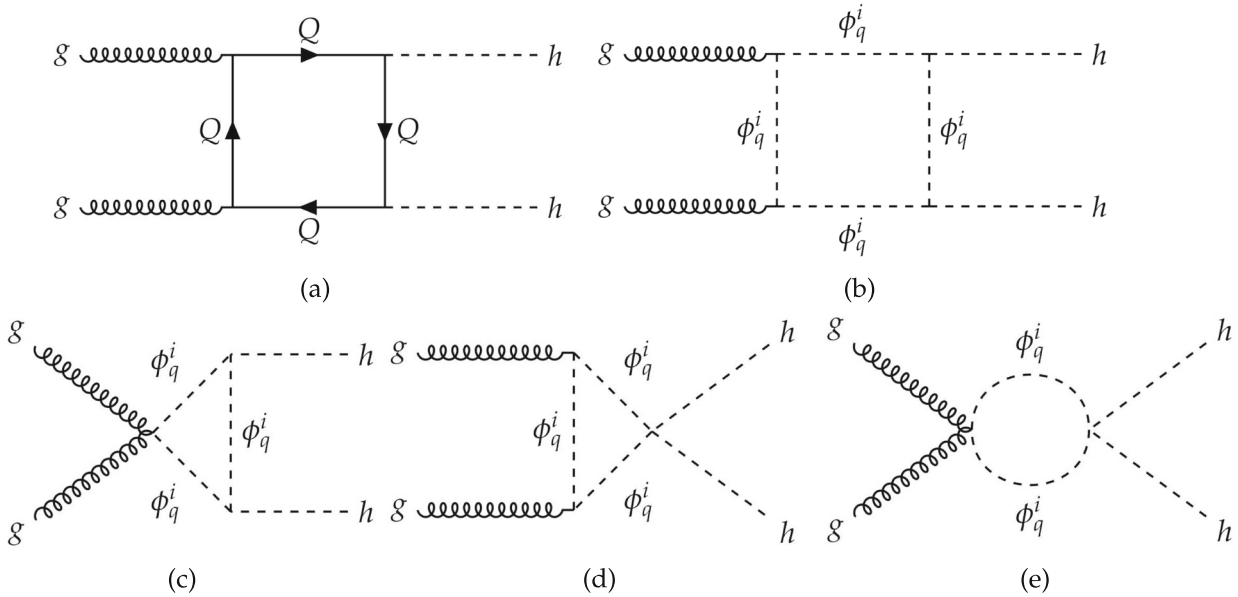


**Fig. 9** Generic diagrams contributing to double Higgs production independent of the trilinear Higgs self-coupling. **a** SM quark loop; **b**–**e** coloured scalar loop

$$-(2m_{\phi_q}^2 + \frac{1}{s}(tu - m_h^4))D_{acb}^{m_{\phi_q}^2}\Big) \tag{35}$$

where we have suppressed the i index only for convenience and

$$F_{\square_2}^{\phi_q^i} = F_{\triangle}^{\phi_q^i}, \tag{36}$$

with the latter given in Eq. (5). Note that, for the same reason we can write this equivalence, we do not have a $G_{\square_2}^{\phi_q^i}$ component, just as for the triangle diagrams ($G_{\square_2}^{\phi_q^i} = G_{\triangle}^{\phi_q^i} = 0$). This is because their amplitudes only differ by the Higgs propagator and constant coupling factors. The Mandelstam variables $s, t, u$ and the scalar integrals $C_{ij}$ and $D_{ijk}$ are defined in the appendix.

### 3.2 The leading-order cross section

The amplitude squared for the computation of the cross section can be separated into two different parts, one for each spin projection,[13] so that the differential partonic cross section can be cast into the form

$$\frac{d\hat{\sigma}^{hh}}{d\hat{t}} = \frac{G_F^2\alpha_s^2}{256(2\pi)^3}\left[|\mathcal{M}_F|^2 + |\mathcal{M}_G|^2\right], \tag{37}$$

where $G_F$ denotes the Fermi constant, $\alpha_s$ the strong coupling constant, and $\hat{t}$ the momentum transfer squared from one of the initial state gluons to one of the final state Higgs bosons. Each of the partial amplitudes $\mathcal{M}_{F/G}$ contains only the terms constructed with the $F/G$ form factors, respectively. Hence

$$\begin{aligned}\mathcal{M}_F = &\sum_Q \left(C_{\triangle}\, g_Q^h F_{\triangle}^Q + C_{\square}\,(g_Q^h)^2 F_{\square}^Q\right)\\ &+\sum_{\phi_q^i}\left(C_{\triangle}\, g_{\phi_q^i}^h F_{\triangle}^{\phi_q^i} + C_{\square}\left((g_{\phi_q^i}^h)^2 F_{\square_1}^{\phi_q^i} + g_{\phi_q^i}^{hh} F_{\square_2}^{\phi_q^i}\right)\right)\end{aligned} \tag{38}$$

[13] The interference term vanishes as for the tensor structures $A_1$ and $A_2$ we have $A_1 \cdot A_2 = 0$.

$$\mathcal{M}_G = C_\square \left( \sum_Q g^h_Q G^Q_\square + \sum_{\phi^i_Q} (g^h_{\phi^i_q})^2 G^{\phi^i_q}_{\square_1} \right). \tag{39}$$

The total cross section for $hh$ production through gluon fusion at the LHC is obtained by integrating Eq. (37) over the scattering angle and the gluon luminosity,

$$\sigma(pp \to hh) = \int_{4m_h^2/s}^1 \mathrm{d}\tau_h \frac{\mathrm{d}\mathcal{L}^{gg}}{\mathrm{d}\tau_h} \hat{\sigma}^{hh}(\hat{s} = \tau_h s) \tag{40}$$

where $s$ is the c.m. energy at the LHC. The numerical evaluation of the total production cross section is performed at LO with the program HPAIR [77,82] where we have implemented the new form factors. The Fortran code HPAIR was originally written for the SM and the MSSM and calculates the double Higgs production through gluon fusion at LO and NLO in the heavy quark limit.

Also for double Higgs production we present our results as a ratio with respect to the SM value in order to minimise the contribution of HO effects, that is $\delta_{hh}$ is defined as

$$\delta_{hh} = \frac{\sigma_{NP} - \sigma_{SM}}{\sigma_{SM}}. \tag{41}$$

This assumes that the HO corrections in our model do not differ significantly from those of the SM, which is a rather good approximation for the QCD corrections.[14,15] The reason is that large differences in the NP and SM QCD corrections are expected to occur at thresholds of the virtual particles. It can be inferred from the comparison of the results on NLO QCD corrections including the full top quark mass dependence with the heavy top limit, that the latter is an approximation, that works rather well for the inclusive cross section. As the NLO QCD corrections are dominated by the real corrections, finite mass effects do not play the dominant role, so that this conclusion should also apply to squark loops. Turning now to the effect of EW corrections: EW corrections in the SM have shown to be rather small, of the order of a few percent [100–106]. Combined with the fact that we investigate relative deviations, the impact of the EW corrections due to new colored scalars should be subleading.

In contrast to single Higgs production we cannot find a simple analytic formula for this quantity due to the more involved form of the amplitudes and consequently also of the cross sections and the dependence of the form factors on the c.m. energy.

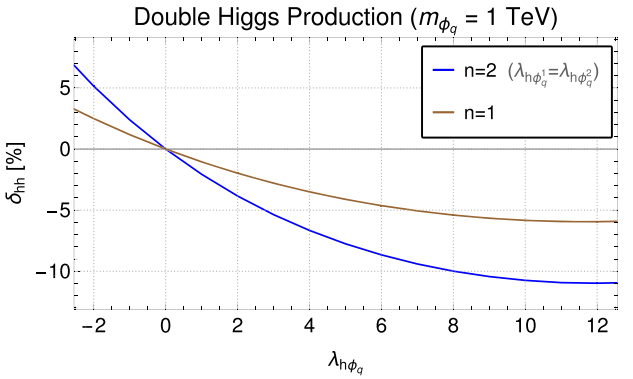


**Fig. 10** $\delta_{hh} = (\sigma_{NP} - \sigma_{SM})/\sigma_{SM}$ as a function of the effective portal coupling $\lambda_{h\phi_q}$ for a mass of $m_{\phi_q} = 1$ TeV and for $n = 1$ and $n = 2$

### 3.3 Phenomenological analysis of the cases $n = 1$ and $n = 2$

Let us start with the simpler scenarios with one or two coloured scalars. The dependence of the form factors on the mass is not trivial. Since the NP contributions should decouple from the SM for very large masses this means that $\delta_{hh}$ would eventually behave as a strictly decreasing function of the coloured scalar mass.

We will follow the same approach as for single Higgs production and choose all coloured scalar masses equal to be 1 TeV. As for the couplings, while in single Higgs production with equal masses only the total sum of the couplings was relevant, in di-Higgs production the amplitude now depends on $\lambda_{h\phi_q^k}$ and $\lambda^2_{h\phi_q^k}$ terms. For now we will impose the constraint of equal couplings for $n = 2$. In Fig. 10 we present $\delta_{hh}$ as a function of the effective portal coupling $\lambda_{h\phi_q}$ for a mass of $m_{\phi_q} = 1$ TeV and for $n = 1$ and $n = 2$. The double Higgs cross section was calculated with HPAIR for a c.m. energy of 14 TeV. As expected, for $\lambda_{h\phi_q} = 0$ the NP and SM LO cross sections coincide, where the SM LO cross section calculated with HPAIR amounts to 16.37 fb.

In Fig. 11 we now present $\delta_{hh}$ as a function of the coloured scalar mass for the minimum (left) and maximum (right) value of the effective portal coupling $\lambda_{h\phi_q}$ and for $n = 1$ and $n = 2$.[16] As expected, the models share similar behaviours when reducing the $n = 2$ case to a single coupling and mass under the equal parameters constraints which approximately double the cross section for two coloured scalars relative to the $n = 1$ scenario. Since $\delta_{hh}$ depends generally on powers of $(\lambda_{h\phi_q})^p$ with $1 \le p \le 4$, this is an indication that the

[14] For the SM, the NLO QCD corrections in the heavy-top limit, including the full top-quark mass dependence at LO, can be found in [82], while the full top quark mass dependence has been provided in [83–87]. The NNLO corrections have been obtained in the heavy-top limit [88,89], the results at next-to-next-to-leading logarithmic accuracy (NNLL) became available in [90,91], and the corrections up to N$^3$LO were presented in [92–95] for the heavy top-mass limit. For a review of higher-order corrections to SM di-Higgs production, see e.g. [96].

[15] For coloured scalars, specifically in the case of the MSSM, the corrections can be found in [82,97–99].

[16] Note that $\delta_{hh}$ has a different sign behaviour than $\delta_h$ as a function of $\lambda_{h\phi_q}$. This is a consequence of the destructive interference between trilinear and box diagrams. For details, see the discussion in Sect. 4.

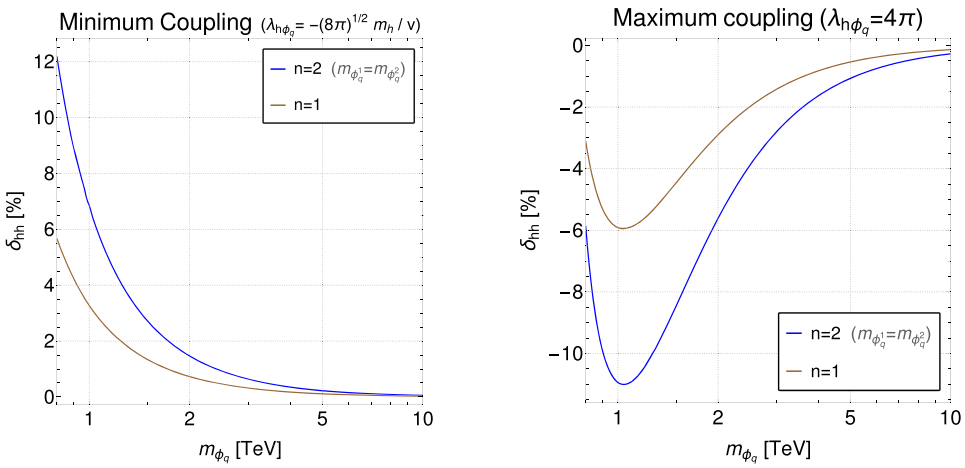


**Fig. 11** $\delta_{hh} = (\sigma_{NP} - \sigma_{SM})/\sigma_{SM}$ as a function of the coloured scalar mass for the minimum value of the coupling (left) and maximum value of the coupling (right) and for $n = 1$ (brown) and $n = 2$ (blue). The double Higgs cross section was calculated with HPAIR for a c.m. energy of 14 TeV

linear terms seem to be the most significant ones for these results - doubling the couplings approximately doubles the cross section. Linear terms can only originate from the diagrams proportional to $\lambda_{h\phi_q}$ and their interference with the SM ones. This is further supported by the observation that, when $\lambda_{h\phi_q} > 0$, the contributions to the Higgs pair production cross section are negative and, hence, odd powers of the coupling are involved. On the other hand, the shape of $\delta_{hh}$ is clearly described by a non-linear function in $\lambda_{h\phi_q}$. Contrary to what happened in single Higgs production, this is no longer necessarily a sign that the interference terms are insufficient to describe the results. This is due to the fact that a dependence on $\lambda^2_{h\phi_q}$ can originate from either the square of the purely NP diagrams proportional to $\lambda_{h\phi_q}$ (see diagrams 8b, c, 9d, e) or from the SM interference with the NP diagrams proportional to $\lambda^2_{h\phi_q}$ (see diagrams 9b, c). The interference term depends on $\sum_k (\lambda_{h\phi_q^k})^2$, while the term originating from squaring the NP diagrams depends on $(\sum_k \lambda_{h\phi_q^k})^2$. For $n = 1$ the two dependencies are identical while for $n \geq 2$ the former represents an extra degree of freedom for $\delta_{hh}$ for a fixed $\sum_k \lambda_{h\phi_q^k}$. This is an important observation if we want to present the results as a function of the sum of the couplings, $\sum_k \lambda_{h\phi_q^k}$, as we did in the single Higgs case.

HPAIR has further been altered with the option to turn on or off particular sets of diagrams. Naturally, we will separate the ones proportional to $\lambda_{h\phi_q}$ and $\lambda^2_{h\phi_q}$. We further separate the two pairs of diagrams 8b, c and 9d, e, since their form factors are the same as in single Higgs production. The sets of diagrams chosen serve the purpose of separating the contributions of the form factors $F^{\phi_q}_{\triangle}$, $F^{\phi_q}_{\square_2}$, which are linear in $g^h_{\phi_q}$ and $g^{hh}_{\phi_q}$, respectively, and $F^{\phi_q}_{\square_1}$ and $G^{\phi_q}_{\square_1}$, which are proportional to the squared coupling $(g^h_{\phi_q})^2$.

The results for $n = 2$ are presented in Fig. 12 for a fixed mass of 1 TeV as a function of the coupling (top), for the minimum coupling as a function of the mass (middle) and for the maximum coupling as a function of the mass (bottom). The left plots show the individual contributions and the interference terms while the right plots present how the individual contributions behave with the couplings (top) and with the mass (middle and bottom). The black line represents the sum of all contributions, while the coloured lines represent the individual coloured scalar form factor contributions, separated as indicated by the legend. Note that the SM contributions drop out in $\delta_{hh}$. More specifically, the contributions denoted by the different colours are proportional to the following coloured form factors and couplings,

$$
\begin{aligned}
&\text{blue}/F_{\triangle}: && \sim \{F^{\phi_q}_{\triangle}, |F^{\phi_q}_{\triangle}|^2\} && \sim \{G^h_{\phi_q}, (G^h_{\phi_q})^2\}\\
&\text{red}/F_{\square_2}: && \sim \{F^{\phi_q}_{\square_2}, |F^{\phi_q}_{\square_2}|^2\} && \sim \{G^{hh}_{\phi_q}, (G^{hh}_{\phi_q})^2\}\\
&\text{green}/F_{\square_1} + G_{\square_1}: && \sim \{F^{\phi_q}_{\square_1}, G^{\phi_q}_{\square_1}, |F^{\phi_q}_{\square_1}|^2, |G^{\phi_q}_{\square_1}|^2\} && \sim \{G^{h,2}_{\phi_q}, G^{h,2}_{\phi_q}, (G^{h,2}_{\phi_q})^2, (G^{h,2}_{\phi_q})^2\}\\
&\text{violet}/F_{\triangle} \cdot F_{\square_2}: && \sim 2\text{Re}(F^{\phi_q}_{\triangle} F^{\phi_q *}_{\square_2}) && \sim G^h_{\phi_q} \cdot G^{hh}_{\phi_q}\\
&\text{orange} && && \\
&/(F_{\triangle} + F_{\square_2}) \cdot F_{\square_1}: && \sim \{2\text{Re}(F^{\phi_q}_{\triangle} F^{\phi_q *}_{\square_1}), 2\text{Re}(F^{\phi_q}_{\square_1} F^{\phi_q *}_{\square_2})\} && \sim \{G^h_{\phi_q} \cdot G^{h,2}_{\phi_q}, G^{h,2}_{\phi_q} \cdot G^{hh}_{\phi_q}\}
\end{aligned}
\tag{42}
$$

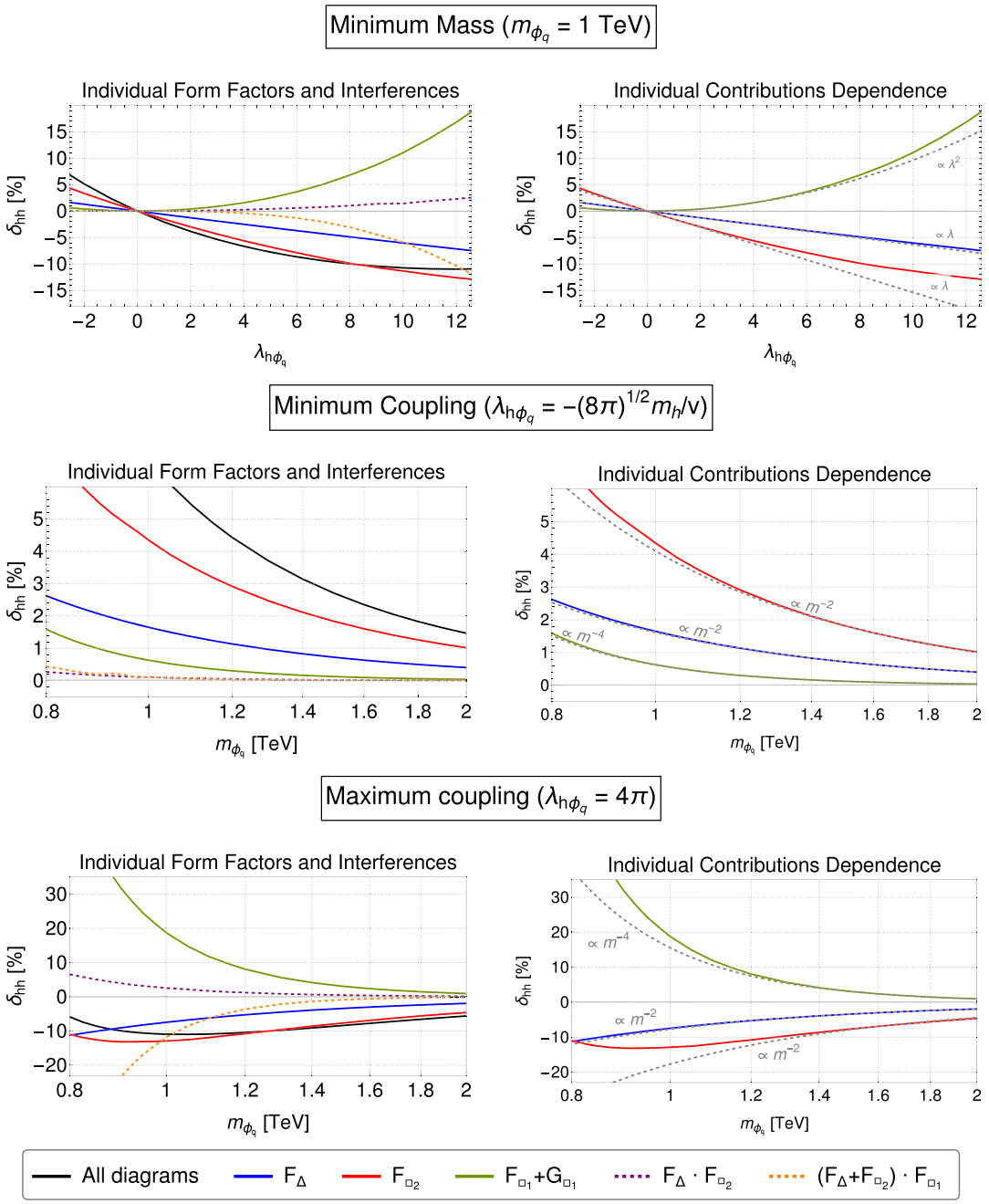


**Fig. 12** $\delta_{hh}$ for $n = 2$ and a fixed mass of 1 TeV as a function of the coupling (top), for the minimum coupling as a function of the mass (middle) and for the maximum coupling as a function of the mass (bottom). Left: individual coloured form factor contributions and interference terms. Right: dependence of the individual contributions on the couplings (top) and the masses (middle and bottom). Black line: sum of all contributions; coloured lines: individual coloured scalar form factor contributions, separated as indicated by the legend and described in Eq. (42). The dashed lines are for the interference terms. Grey dashed lines: asymptotic behaviour in the scenario where the interference terms with the SM are the dominant ones. The grey full line at 0 in all plots is there to guide the eyes

where we introduced the abbreviations

$$G^h_{\phi_q} \equiv \sum_{\phi^i_q} \frac{\lambda_{h\phi^i_q} v}{2m^2_{\phi^i_q}}, \quad G^{hh}_{\phi_q} \equiv \sum_{\phi^i_q} \frac{\lambda_{h\phi^i_q}}{2m^2_{\phi^i_q}},$$

$$G^{h,2}_{\phi_q} \equiv \sum_{\phi^i_q} \left( \frac{\lambda_{h\phi^i_q} v}{2m^2_{\phi^i_q}} \right)^2 . \tag{43}$$

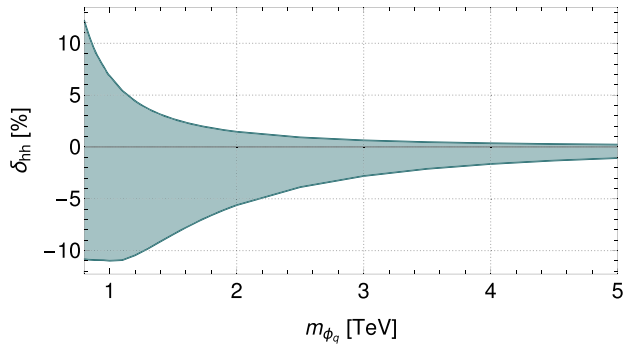


**Fig. 13** $\delta_{hh}$ as a function of the scalar mass $m_{\phi_q}$ for $n = 2$. The couplings are varied between the two extreme values as discussed previously. Above $m_{\phi_q} = 1$ TeV the minimum is obtained at the maximum values for the couplings and the curve follows Fig. 11, while below this mass the couplings are not equal, resulting in the different observed behavior

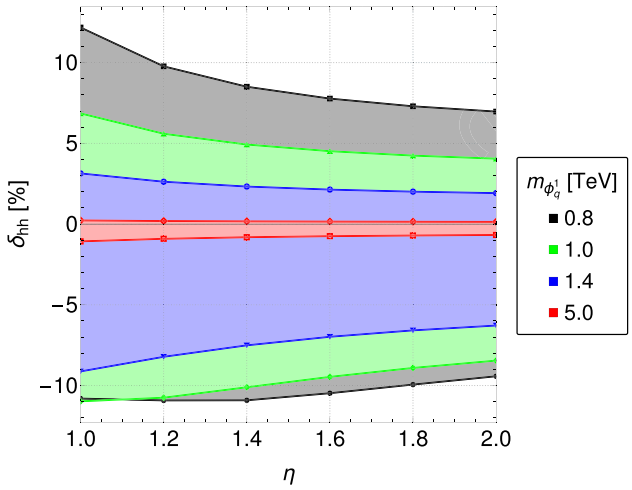


**Fig. 14** $\delta_{hh}$ as a function of the variable $\eta$ defined as $m_{\phi_q^2} = \eta\, m_{\phi_q^1}$. The plot is for $n = 2$ and $\eta$ was varied between 1 and 2. This relaxes the condition of equal masses fixing $m_{\phi_q^1}$ while increasing $m_{\phi_q^2}$. The different colours represent the different values for the fixed mass, $m_{\phi_q^1}$

Note that $G^{hh}_{\phi_q}$ and $G^{h}_{\phi_q}$ only differ by a factor $1/v$. The terms linear in the form factors of the blue, red and green contribution stem from the interference with the SM form factors. The violet and orange contributions (dashed lines) hence denote the interference terms between the coloured contributions. The grey dashed lines in the right plots show the asymptotic behaviour in the coupling (top) and the coloured masses (middle/bottom) in the scenario where the interference terms with the SM are the dominant ones (where we generically denote by $\lambda$ the couplings $G^{h}_{\phi_q}$ (blue line) and $G^{hh}_{\phi_q}$ (red line) and by $\lambda^2$ the coupling $G^{h,2}_{\phi_q}$ (green line)). We can infer from the three plots that for masses of 1 TeV and higher and for any coupling values, both the $F_\triangle$ (blue line) and the $F_{\square_1} + G_{\square_1}$ (green line) contributions are rather well described by only considering their interference with the SM form factors. The $F_{\square_2}$ contribution (red line), however, is not well approximated by the interference with the SM contribution only (for the smaller masses and large couplings).

We end this section by presenting in Fig. 13 the double Higgs corrections $\delta_{hh}$ as a function of the scalar mass $m_{\phi_q}$ for $n = 2$. The couplings are varied between the two extreme values as discussed previously. The new physics impact due to the additional coloured loops are below 10 % already for a mass of 1 TeV and fall steeply with rising mass. Therefore the effect of two extra coloured scalar only will be extremely hard to probe even at the HL-LHC.

### 3.4 Model $n = 2$ for different masses

We very briefly look at the implications of relaxing the condition of equal masses. For this, we calculated the full range of $\delta_{hh}$ for ratios between the two masses of

$$m_{\phi_q^2} = \eta\, m_{\phi_q^1} \tag{44}$$

while scanning over all values for the couplings. Using `HPAIR`, the results for $\delta_{hh}$ are displayed in Fig. 14. The plot is for $n = 2$ and $\eta$ was varied between 1 and 2 and we find similar conclusions to the ones discussed in the previous section. There, we found that, when increasing the two masses equally above 1 TeV, the range of values for $\delta_{hh}$ would always shrink. Naturally, when increasing only one mass, we expect the same to happen, although the effect is milder as can be seen in the figure. We have checked that for $n = 2$,

$$\delta_{hh}^{\max/\min}(m_{\phi_q^1}, m_{\phi_q^2}) \approx \big[\delta_{hh}^{\max/\min}(m_{\phi_q^1}, m_{\phi_q^1}) + \delta_{hh}^{\max/\min}(m_{\phi_q^2}, m_{\phi_q^2})\big]/2. \tag{45}$$

This is a consequence of the more general observation that

$$\delta_{hh}(m_{\phi_q^1}, m_{\phi_q^2}, \lambda_{h\phi_q}) \approx \big[\delta_{hh}(m_{\phi_q^1}, m_{\phi_q^1}, \lambda_{h\phi_q}) + \delta_{hh}(m_{\phi_q^2}, m_{\phi_q^2}, \lambda_{h\phi_q})\big]/2. \tag{46}$$

We can conclude that relaxing the equal masses condition will not result in any additional behaviour of note. Reducing one mass has the same effect as reducing both but with the obvious difference that the effect is less significant. Consequently, we will also not obtain a larger range of values for $\delta_{hh}$ by adding this extra freedom. We can now extrapolate this conclusion for higher values of $n$. This scenario will be discussed in the next section.

### 3.5 Models with $n$ coloured scalars

We finalise this chapter by looking in more detail at double Higgs production in the case of an arbitrary number of scalars. The parameter space will be comprised of $n$ effective couplings $\lambda_{h\phi_q^k}$ to the Higgs boson and $n$ scalar masses

$m^2_{\phi_q^k}$ ($k = 1, \ldots, n$), one for each of the coloured scalars, resulting in $2n$ input parameters ( $\lambda_k \equiv \lambda_{h\phi_q^k}$ from now on).

We again start with the condition of equal masses, $m^2_{\phi_q^k} = m^2_{\phi_q^l} \equiv m^2_{\phi_q}$, reducing the input parameters to $n+1$. As discussed in the previous section, this condition should be sufficient in order to fully explore $\delta_{hh}$. For single Higgs production, this resulted in a simple dependence of the corrections on only the total sum of the couplings. In the case of Higgs pair production, the amplitude now contains both $\lambda_k$ and $\lambda_k^2$ terms and thus there are now two relevant quantities: the total sum of the couplings and the total sum of the squared couplings. Naturally, taking these two sums over the couplings as our parameters is advantageous, as it allows us to reduce the number of input parameters from $n+1$ to only 3, to properly study $\delta_{hh}$ for any model. The cases $n = 1, 2$ have two and three independent input parameters, respectively, and were studied in the previous sections.

We will now proceed to write both the cross section $\sigma_{hh}$ and the relative deviation from the SM cross section, $\delta_{hh}$, as a function of the two effective quantities, $\sum \lambda_k$ and $\sum \lambda_k^2$. Assuming a common fixed coloured mass $m^2_{\phi_q}$, as we do from now on, we note that because single Higgs production only depends on $\sum \lambda_k$, if one is able to write the relative deviations $\delta_{h,hh}$ as a function of the same variable, the two results can be combined. Even under the simplification of equal masses, we have now $\delta_{hh}$ as a function of two parameters, $\delta_{hh} \equiv \delta_{hh}\left(\sum \lambda_k, \sum \lambda_k^2\right)$. Therefore, the model limits are represented by a 2-dimensional region in the parameter space of these two sums. By taking the approach where we consider the sum $\sum \lambda_k$ as the independent variable, the limits on this sum are easily obtained. Applying the same constraints, $\lambda_{min} \leq \lambda_k \leq \lambda_{max}$, to all the couplings of a model with $n$ coloured scalars, the sum of the couplings will be limited by

$$n\lambda_{min} \leq \sum \lambda_k \leq n\lambda_{max}. \tag{47}$$

As for the limits for $\sum \lambda_k^2$ as a function of $\sum \lambda_k$, we need to find the solution of a conditional extreme problem: the extremes of $\sum \lambda_k^2$ subject to the constraints $\sum \lambda_k = c$ and $\lambda_{min} \leq \lambda_k \leq \lambda_{max}$. Within the $n$ dimensional space of the individual couplings, $(\lambda_1, \lambda_2, \ldots \lambda_n)$, the region of interest is represented by an $n-1$ hyperplane defined by $\sum \lambda_k = c$ but constrained by an $n$-dimensional hypercube resulting from the constrained couplings, $\lambda_{min} \leq \lambda_k \leq \lambda_{max}$. For a fixed sum ($\sum \lambda_k = c$) the minimum of $\sum \lambda_k^2$ is given when the couplings are all equal

$$\sum \lambda_k^2 \geq \frac{c^2}{n} = \frac{\left(\sum \lambda_k\right)^2}{n} \tag{48}$$

which is a just a Cauchy–Schwartz type of inequality.

The determination of the maximum is more elaborated. The solution is given by the edges of the hypercube or, more simply, when all but one coupling are fixed to $\lambda_{min}$ or $\lambda_{max}$. This can be cast in the form,

$$\begin{aligned}\sum_{k=1}^{n} \lambda_k^2 \leq \sum_{j=0}^{n-1} \Bigg\{ \Bigg[ & j\lambda_{max}^2 + (n-1-j)\,\lambda_{min}^2 \\ & + \left(\sum_{k=1}^{n} \lambda_k - (j\lambda_{max} + (n-1-j)\,\lambda_{min})\right)^2 \Bigg] \\ & \times \left[\Theta\left(\sum_{k=1}^{n} \tilde{\lambda}_k - j\right) - \Theta\left(\sum_{k=1}^{n} \tilde{\lambda}_k - (j+1)\right)\right]\Bigg\}\end{aligned} \tag{49}$$

where $\tilde{\lambda}_k = (\lambda_k - \lambda_{min})/(\lambda_{max} - \lambda_{min})$ and $\Theta(x)$ is the Heaviside function. The derivation of this formula can be found in [107].

In Fig. 15 we present an example of the region determined by the above conditions. We show the allowed regions for each model defined by the number $n$ of coloured scalars. The left plot depicts the borders of the labelled regions for even values of $n$. The odd values in-between are represented by a dashed grey line. The right plot focuses on the lower values of $n$, representing all up to $n = 4$. Higher values are represented by grey dashed lines.

The next step is to calculate $\delta_{hh}$ as a function of the two sums $\sum \lambda_k$ and $\sum \lambda_k^2$. This can be done by discretising the two variables in $N$ points which would involve a computational time of $\mathcal{O}(N^2)$. We will instead present an approach that can recycle the previous results from Fig. 12 with $n = 2$ and a fixed mass, which can be computed in $\mathcal{O}(N)$ time. We separate the individual contributions to $\delta_{hh}$ into three components as follows:

$$\begin{aligned}
\delta^{\,A}_{n,\,\mathrm{eq}}(\lambda) &: \sim \{F_{\triangle}^{\phi_q}, |F_{\triangle}^{\phi_q}|^2, F_{\square_2}^{\phi_q}, |F_{\square_2}^{\phi_q}|^2, 2\mathrm{Re}(F_{\triangle}^{\phi_q} F_{\square_2}^{\phi_q *})\} \sim \{G^h_{\phi_q}, (G^h_{\phi_q})^2, G^{hh}_{\phi_q}, (G^{hh}_{\phi_q})^2, G^h_{\phi_q} \cdot G^{hh}_{\phi_q}\} \\
\delta^{\,B}_{n,\,\mathrm{eq}}(\lambda) &: \sim \{F_{\square_1}^{\phi_q}, G_{\square_1}^{\phi_q}, |F_{\square_1}^{\phi_q}|^2, |G_{\square_1}^{\phi_q}|^2\} \sim \{G^{h,2}_{\phi_q}, G^{h,2}_{\phi_q}, (G^{h,2}_{\phi_q})^2, (G^{h,2}_{\phi_q})^2\} \\
\delta^{\,C}_{n,\,\mathrm{eq}}(\lambda) &: \sim \{2\mathrm{Re}(F_{\triangle}^{\phi_q} F_{\square_1}^{\phi_q *}), 2\mathrm{Re}(F_{\square_1}^{\phi_q} F_{\square_2}^{\phi_q *})\} \sim \{G^h_{\phi_q} \cdot G^{h,2}_{\phi_q}, G^{h,2}_{\phi_q} \cdot G^{hh}_{\phi_q}\}
\end{aligned} \tag{50}$$

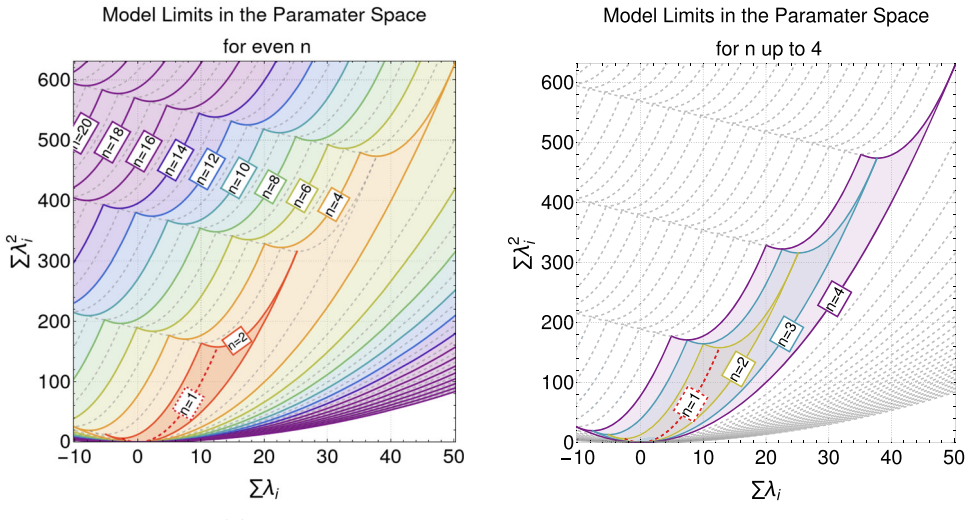


**Fig. 15** Allowed regions for each model defined by the number $n$ of coloured scalars. The left plot depicts the borders of the labelled regions for even values of $n$. The odd values in-between are represented by a dashed grey line. Of note is that, for $n = 1$, the limits are not a region but just a single line (represented as a dashed red line). The right plot focuses on the lower values of $n$, representing all up to $n = 4$. Higher values are represented by grey dashed lines

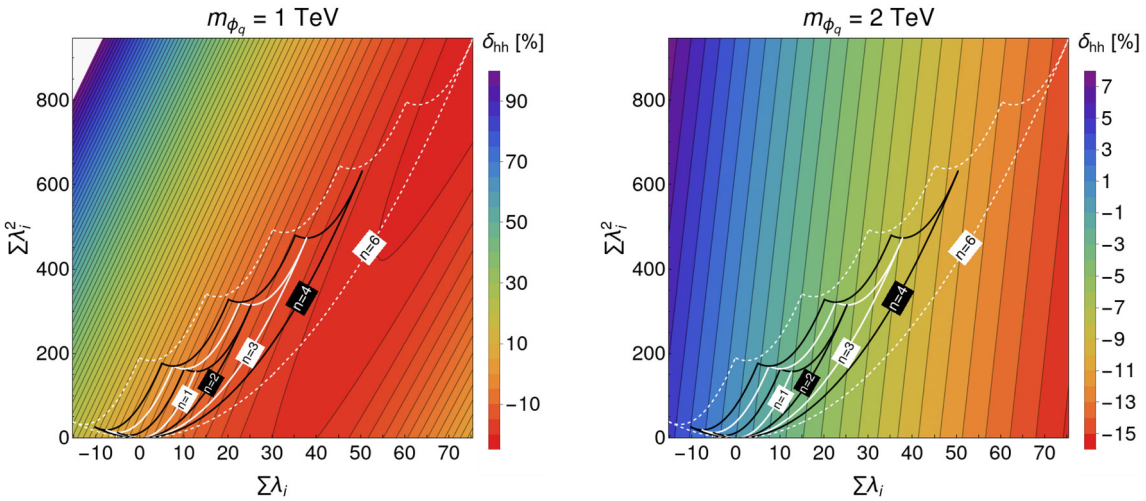


**Fig. 16** $\Sigma\lambda_i^2$ as a function of $\Sigma\lambda_i$ with the value of $\delta_{hh}$ in the colour bar. Left (right): $m_{\phi_q} = 1(2)$ TeV. Note that the colour scale is not the same in the two figures. The contours represent the allowed values for $\delta_{hh}$ for each value of $n$. The allowed region for $n = 5$ has not been represented as it would make the identification of the $n = 4$ and $n = 6$ regions more difficult

where the label "eq" indicates the equal coupling condition ($\lambda_k = \lambda_l \equiv \lambda$) and there is only one independent parameter, $\lambda$, due to this condition. We have already found that all three components can be significant and must be taken into account. The equivalence between these three components for a model with $n$ couplings with an arbitrary model with $n'$ couplings, $\{\lambda'_1, \ldots, \lambda'_{n'}\}$, is given by the following formula:

$$\begin{aligned}\delta_{hh}^{n'}(\{\lambda'_1,\ldots,\lambda'_{n'}\}) &= \delta^A_{n,\,\mathrm{eq}}(\lambda)\Big|_{\lambda=\frac{1}{n}\sum\lambda'_k} + \delta^B_{n,\,\mathrm{eq}}(\lambda)\Big|_{\lambda=\sqrt{\frac{1}{n}\sum\lambda'^2_k}} \\ &+\delta^C_{n,\,\mathrm{eq}}(\lambda)\Big|_{\lambda=\sqrt[3]{\left(\frac{1}{n}\sum\lambda'_k\right)\left(\frac{1}{n}\sum\lambda'^2_k\right)}}. \end{aligned} \tag{51}$$

In other words, the $\delta_{hh}^{n'}$ for a model with $n'$ couplings can be obtained from the results for a model with $n$ equal couplings $\lambda$, by taking the $A$, $B$, and $C$ contributions at the $\lambda$ values indicated by the vertical bars.

In Fig. 16 we show $\Sigma\lambda_i^2$ as a function of $\Sigma\lambda_i$ with the value of $\delta_{hh}$ in the colour bar. The left plot is for a coloured scalar mass of 1 TeV while the right plot is for 2 TeV. Note that the colour scale is not the same in the two figures. The contours represent the allowed values for $\delta_{hh}$ for each value of $n$. The comparison of the two plots shows that, as expected, the range of variation of $\delta_{hh}$ decreases with increasing value of $m_{\phi_q}$. Furthermore, the dependence of $\delta_{hh}$ on $\sum\lambda_k^2$ decreases with increasing coloured mass which is due to the fact that

the terms proportional to $\sum \lambda_k^2$ are suppressed by a factor of $1/m_{\phi_q}^4$.

In Fig. 17 we now show $\delta_{hh}$ as a function of the sum of couplings, $\sum \lambda_k$. The range of variation is related with the freedom in $\sum \lambda_k^2$ and was calculated with the results and model limits from Fig. 16. As the mass grows the term in $\lambda_k$ becomes increasingly important and for a mass of 2 TeV the variation in $\lambda_k^2$ almost vanishes. Therefore, for large masses the dependence for single and double Higgs productions becomes very similar. Note, that since the interference is destructive for positive couplings in the case of double Higgs production, the maximum $\delta_{hh}$ occurs for the smaller (negative) values of the couplings.

Finally, in Fig. 18 left (right) we present $\delta_{hh}$ as a function of the number of scalars $n$ for three (five) coloured scalar masses. The left plot shows the scenarios from $n = 1$ to $n = 10$ while the right plot shows larger values of $n$. For small $n$ the deviations from the SM are small as we had seen before but they can be extremely large for very large values of $n$, even if the coloured scalar masses are large.

Contrary to single Higgs production, the experimental limits on double Higgs production are very weak and at the moment unlikely to be useful in constraining the parameter space. The lowest observed bound on the limit for double Higgs production, as reported by the ATLAS collaboration to be 2.4 times the SM cross section, is equivalent to a $\delta_{hh}$ of 140% [108] for a c.m. energy of 13 TeV. With a mass of 1 TeV, this would apply constraints only above $n \approx 24$. As for possible future improvements we can consider the HL-LHC projections [74]. For the $hh \to b\bar{b}b\bar{b}$ channel a reported value as low as 1.6 times the SM cross section, equivalent to a $\delta_{hh}$ of 60%, can be achieved, assuming that the overall uncertainty scales with the luminosity as $1/\sqrt{L}$. This would bring the previous threshold value of $n$ down to around 13. This means that certain combinations of the masses with the number of scalars will certainly be constrained with future measurements.

## 4 Single Higgs vs. double Higgs production

In the previous chapters we have discussed in detail the contribution of an arbitrary number of coloured scalars to single Higgs and di-Higgs production processes via gluon fusion at the LHC. We will now discuss the complementarity between the two processes. One should note, however, that although we expect a good precision in the measurement of the single Higgs process this is not the case for di-Higgs production.

The first point to note is that the NP contribution to the single Higgs mode has a constructive interference for positive $\lambda_k$ while for di-Higgs it is negative. The reason for the positive interference term for $\lambda_k > 0$, is that both the SM and the NP form factors in single Higgs production are positive. For double Higgs production this is no longer the case. The reason behind this is the destructive interferences between the $(F_\triangle^{Q/\phi_q}, F_{\square_2}^{\phi_q})$ and $(F_\square^Q, F_{\square_1}^{\phi_q})$ form factors. It is already well known that the SM triangle and box form factors interfere destructively as can be read off from their values in the heavy quark limit, $F_\triangle^Q = \frac{2}{3} + \mathcal{O}(m_Q^{-2})$ and $F_\square^Q = -\frac{2}{3} + \mathcal{O}(m_Q^{-2})$. To understand why this also applies to our coloured scalars we can make use of the low-energy theorem, applied e.g. in [52,56,80,97,109–111], to deduce the sign of $F_{\square_1}^{\phi_q}$. By applying this theorem, one can show that $F_{\square_1}^{\phi_q}$ is given by the derivative in mass of the term $F_\triangle^{\phi_q}/m_{\phi_q}^2$. Since we already know that the triangle form factor for large scalar masses decreases with the mass, the sign of $F_{\square_1}^{\phi_q}$ will be negative. Therefore the negative contributions for positive couplings we are observing are due to the interference terms of the NP form factors, $F_\triangle^{\phi_q} \cdot F_{\square_1}^{\phi_q}$ and $F_{\square_2}^{\phi_q} \cdot F_{\square_1}^{\phi_q}$, but also from the interference between SM and NP form factors, $F_\square^Q \cdot F_\triangle^{\phi_q}$, $F_\square^Q \cdot F_{\square_2}^{\phi_q}$ and $F_\triangle^Q \cdot F_{\square_1}^{\phi_q}$. The remaining $F \cdot F$ terms involving at least one NP form factor are positive. As for $G_\square^Q \cdot G_{\square_1}^{\phi_q}$, its contribution to the amplitude is suppressed by $(1/m_Q^2) \cdot (1/m_{\phi_q}^6)$, where the latter factor stems from the $G_{\square_1}^{\phi_q}$ dependence $\sim 1/m_{\phi_q}^2$ multiplied by the coupling factor $(g_{\phi_q}^h)^2 \sim 1/m_{\phi_q}^4$.

In Fig. 19 we present $\delta_{hh}$ (blue) and $\delta_h$ (brown) as a function of the averaged coloured coupling $\sum \lambda_k/n$ for $n = 1$ (left) and $n = 2$ (right). The mass of the coloured scalars has been chosen equal and set to 1 TeV. We note that with the chosen input values given above we obtain at $\sqrt{s} = 14$ TeV at LO for the SM the single Higgs cross section value $\sigma_{SM}^h = 15.76$ pb calculated with `HIGLU` including the bottom, charm and top quark loops, and the double Higgs cross section value $\sigma_{SM}^{hh} = 16.37$ fb calculated with `HPAIR` including the bottom and top quark loops. The complementarity between the dependence of $\delta_h$ and $\delta_{hh}$ w.r.t. the coupling $\lambda_k$ is very clear from the figure. We also note that for $n = 1$ the $\delta_h$ and $\delta_{hh}$ values are lines while for $n = 2$ there is an allowed region for $\delta_{hh}$ due to the additional dependence on $\sum_k \lambda_k^2$. This leads to the observation that, with a single Higgs measurement very close to the SM value constraining $\sum \lambda_k/n$ to small values, any significant excess of di-Higgs production would provide a strong indication that $n \geq 2$.

We finalise this section with a plot (Fig. 20) where we show the region of the coloured mass versus the number of scalars that leads to a maximal deviation of 1.6% in $\delta_h$ (left) and to a maximal deviation of 60% in $\delta_{hh}$ (right) of single, respectively, double Higgs production from the corresponding SM value, while varying the couplings within their allowed theoretical bounds. The limits correspond to the HL-LHC projections [74] and thus the plots give us an idea of the region where it will not be possible to probe these models. We can only apply cuts to the coupling values for masses below this

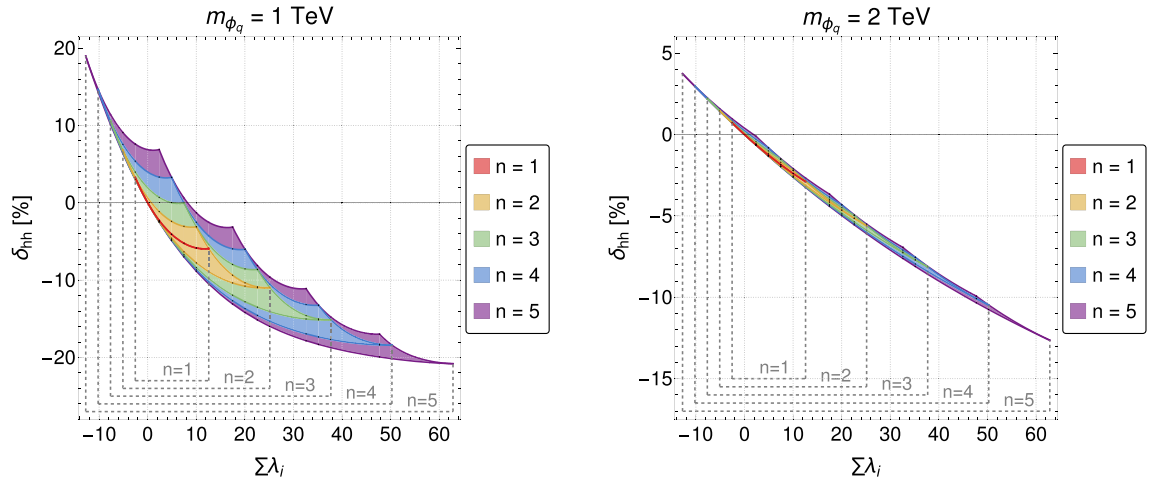


**Fig. 17** $\delta_{hh}$ for a scalar mass of 1 TeV (left) and 2 TeV (right) as a function of $\sum \lambda_i$. This encompasses the possible range from the freedom in $\sum \lambda_i^2$ and was calculated with the results and model limits from Fig. 16

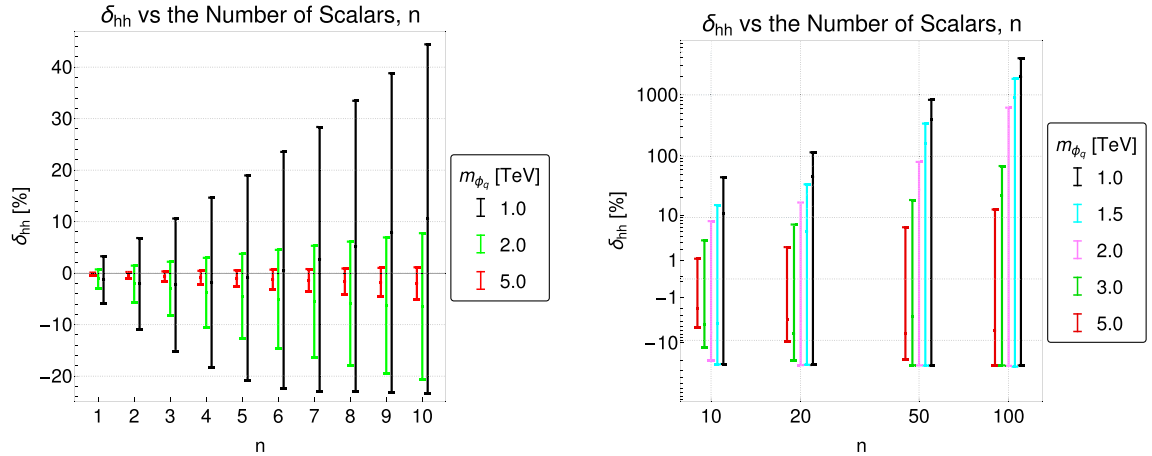


**Fig. 18** The ranges of values for $\delta_{hh}$ as a function of the number of scalars $n$ for three (left) and five (right) coloured scalar masses with $n = 1, \ldots, 10$ (left) and $n = 10, 20, 50, 100$ (right)

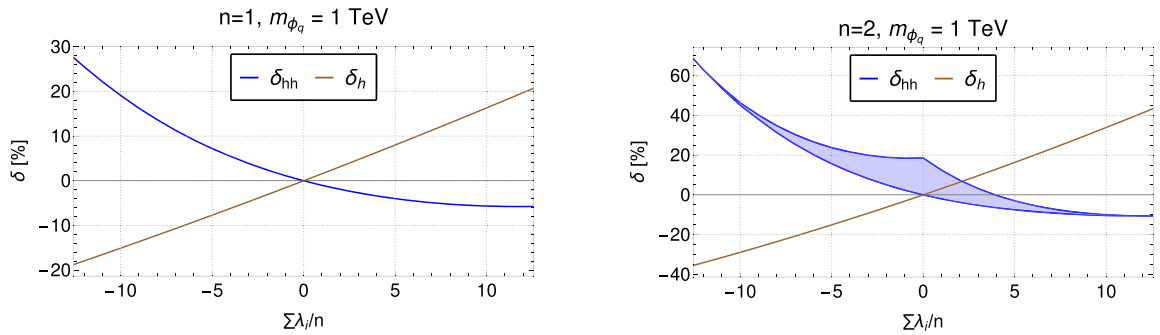


**Fig. 19** $\delta_{hh}$ (blue) and $\delta_h$ (brown) as a function of the averaged coupling for $n = 1$ (left) and for $n = 2$ (right). For these plots only, the minimum coupling used was $-4\pi$ instead of the previous bounded-from-below condition

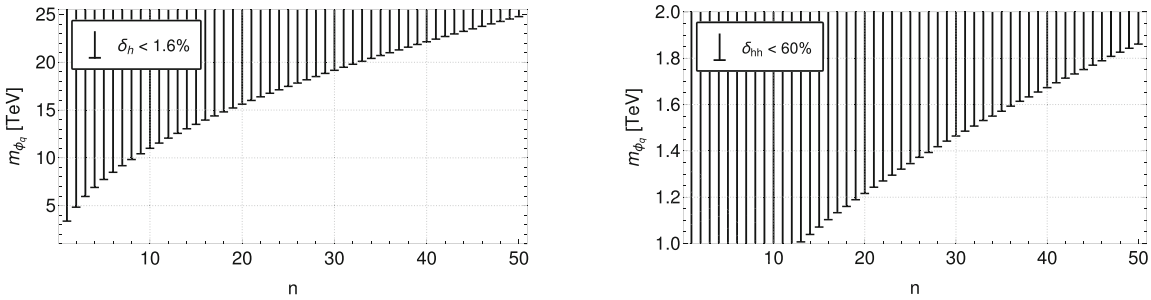


**Fig. 20** Regions where $\delta_h$ (left) and $\delta_{hh}$ (right) fall below 1% as a function of the coloured scalar mass and the number of scalars. For the single Higgs production (left) the threshold of 0.1% has also been included. For these calculations the previous BFB condition from Eq. (20) was used

region. As single Higgs production can be constrained more stringently than Higgs pair production this means that larger coloured masses can be probed in single than in di-Higgs production. Independent of the experimental precisions, the plots show, that single Higgs production is more sensitive to coloured scalars than di-Higgs production. For a value of $n = 20$ e.g. a value of $\delta_h = 1.6\%$ probes masses of about 15 TeV, whereas $\delta_{hh} = 60\%$ probes masses of 1.2 TeV only. Finally, we have checked that the lower border of the single Higgs region, where $\delta_h = 1.6\%$, follows the relationship $n \propto m_{\phi_q}^2$ very closely. The large masses required for these low values of $\delta$ ensure that the terms proportional to $n/m_{\phi_q}^2$ are dominant and hence why this behaviour is observed. For double Higgs production this does not hold as well.

## 5 A more detailed study of the $n = 1$ and $n = 2$ scenarios

The results presented in the previous sections are valid for any type of model with an arbitrary number of independent coloured scalars provided that there is no mixing between them. Also, there is no need to fix the electric charge, or alternatively the hypercharge and isospin, to perform the calculation. It is only when we organise them in isospin multiplets and choose the hypercharge that electric charge will be defined. Hence, the new physics contribution to the electroweak (EW) oblique parameters $S$, $T$ and $U$ [112,113] is model dependent. If we consider the case $n = 1$ the contribution to these parameters is zero, and for $n > 1$ it depends on the group representation of the fields.

Similarly, direct searches at LHC are again very model dependent. The number of possible final states with DM candidates grows with $n$, making our approach more useful for large $n$, since in direct detection the number of final states could be huge. The important point to note is that the contribution of the coloured scalar to loop processes is independent of the specific model under study.

We also note that DM direct detection, DM indirect detection and the constraints from relic density do not apply to these colour-charged scalars. The models have a neutral particle from the dark sector that acts as a DM candidate (see [10,11] for details).

Still we will discuss the particular cases of $n = 1$ and $n = 2$, meaning the $SU(2)_L$ singlet and doublet representation of the coloured scalar field.

### 5.1 Electroweak precision observables

The contribution of new physics to the $T$ parameter, the one relevant in our scenarios, can play an important role in extensions of the SM in restricting the parameter space. In what follows we will discuss the two specific models of Refs. [10,11] corresponding to $n = 1$ and for $n = 2$.

We start by presenting a quick introduction to their contents. The SM is extended with three $Z_2$-odd fields, of which two are scalars, $\Phi_l$ and $\Phi_q$, and one is a vectorlike fermion, $\chi$. The following Yukawa interactions are then added:

$$\mathcal{L} = \cdots + \mathrm{y}_{Q_i} \bar{Q}_{L_i} \Phi_q \chi_R + \mathrm{y}_{L_i} \bar{L}_{L_i} \Phi_l \chi_R + h.c. \tag{52}$$

where the SM left-handed lepton doublet, $L_{L_i}$, is coupled to the $\Phi_l$ scalar while the SM left-handed quark doublet, $Q_{L_i}$, is coupled to the $\Phi_q$ scalar. Because of this, both scalars, $\Phi_l$ and $\Phi_q$, sit in the same $SU(2)_L$ representation but only $\Phi_q$ has colour charge. Yet this is not enough to uniquely determine the $SU(2)_L \times U(1)_Y$ charges for the three fields. Table 1 presents some of the combinations where the scalars are either singlets or doublets. For this section we will study model 5 ($n = 1$) with the three fields cast into the form

$$\chi = \begin{pmatrix} \chi^0 \\ \chi^- \end{pmatrix}, \quad \Phi_l = \frac{1}{\sqrt{2}}(S + iA), \quad \Phi_q = \phi_q^{+2/3}, \tag{53}$$

and the scalar potential given by

$$V^{n=1} = -\mu_H^2 |H|^2 + \lambda_H |H|^4 + \mu_{\Phi_q}^2 |\Phi_q|^2 + \lambda_{\Phi_q} |\Phi_q|^4 + \mu_{\Phi_l}^2 |\Phi_l|^2 + \lambda_{\Phi_l} |\Phi_l|^4$$

**Table 1** Possible variations of the charges for the fields. In every model $\chi_R$ and $\Phi_l$ are singlets of $SU(3)_c$ while $\Phi_q$ is a triplet and the only coloured field

| Model | $\chi_R$ | | $\Phi_l$ | | $\Phi_q$ | |
|---|---|---|---|---|---|---|
| | $SU(2)_L$ | $U(1)_Y$ | $SU(2)_L$ | $U(1)_Y$ | $SU(2)_L$ | $U(1)_Y$ |
| 1 | **1** | 1 | **2** | $-3/2$ | **2** | $-5/6$ |
| 2 | **1** | 0 | **2** | $-1/2$ | **2** | 1/6 |
| 3 | **1** | $-1$ | **2** | 1/2 | **2** | 7/6 |
| 4 | **2** | 1/2 | **1** | $-1$ | **1** | $-1/3$ |
| 5 | **2** | $-1/2$ | **1** | 0 | **1** | 2/3 |

Bold values indicate the representation of the group

$$
\begin{aligned}
&+\frac{\mu'^2_{\Phi_l}}{2}\left(\Phi_l^2+\Phi_l^{*2}\right)+\frac{\lambda'_{\Phi_l}}{4}\left(\Phi_l^2+\Phi_l^{*2}\right)^2\\
&+\frac{\lambda'_{\Phi_q\Phi_l}}{2}|\Phi_q|^2\left(\Phi_l^2+\Phi_l^{*2}\right)+\frac{\lambda'_{H\Phi_l}}{2}|H|^2\\
&\times\left(\Phi_l^2+\Phi_l^{*2}\right)+\lambda_{H\Phi_q}|H|^2|\Phi_q|^2\\
&+\lambda_{H\Phi_l}|H|^2|\Phi_l|^2+\lambda_{\Phi_q\Phi_l}|\Phi_q|^2|\Phi_l|^2. \qquad (54)
\end{aligned}
$$

Whereas for model 3 ($n=2$) we have the fields

$$
\chi=\chi^-,\quad \Phi_l=\begin{pmatrix}\phi_l^+\\ \frac{1}{\sqrt{2}}(S+iA)\end{pmatrix},\quad \Phi_q=\begin{pmatrix}\phi_q^{+5/3}\\ \phi_q^{+2/3}\end{pmatrix}, \qquad (55)
$$

with the scalar potential given by

$$
\begin{aligned}
V^{n=2}=&-\mu_H^2|H|^2+\lambda_H|H|^4+\mu_{\Phi_q}^2|\Phi_q|^2\\
&+\lambda_{\Phi_q}|\Phi_q|^4+\mu_{\Phi_l}^2|\Phi_l|^2+\lambda_{\Phi_l}|\Phi_l|^4\lambda_{\Phi_q\Phi_l}|\Phi_q|^2|\Phi_l|^2\\
&+\lambda_{H\Phi_q}|H|^2|\Phi_q|^2+\lambda_{H\Phi_l}|H|^2|\Phi_l|^2\lambda'_{\Phi_q\Phi_l}|\Phi_q^\dagger\Phi_l|^2\\
&+\lambda'_{H\Phi_q}|H^\dagger\Phi_q|^2+\lambda'_{H\Phi_l}|H^\dagger\Phi_l|^2\Lambda_{\Phi_q\Phi_l}|\Phi_l^\dagger i\sigma_2\Phi_q|^2\\
&+\Lambda_{H\Phi_q}|H^\dagger i\sigma_2\Phi_q|^2+\lambda_5((H^\dagger\Phi_l)^2+(\Phi_l^\dagger H)^2). \qquad (56)
\end{aligned}
$$

For both models the Lagrangian for the vectorlike fermion, $\chi$, is given by

$$
\mathcal{L}_\chi=i\bar{\chi}\gamma^\mu(D_\mu\chi)-m_\chi\bar{\chi}\,\chi. \qquad (57)
$$

For $n=1$, that is, the singlet case, the contribution to $T$ is zero. In this model not only all scalars are $SU(2)_L$ singlets but also both components of the vectorlike fermion have the same mass and therefore there is no contribution to the oblique parameters at one-loop.

For $n=2$ the most relevant contributions to the $T$ parameter are as follows. First, there is no contribution from the singlet vectorlike fermion $\chi$ because its contribution to the vacuum polarization amplitude from the $W$ and $Z$ boson self-energies is similar to the one in QED, which vanishes in the limit of zero momentum transfer. In order to determine the contribution of the scalar fields to $T$ we have used the expression in [114], obtained for an $SU(2)_L\times U(1)$ electroweak model with an arbitrary number of scalar doublets, with hypercharges $\pm1/2$, and also an arbitrary number of scalar singlets. The contribution to $T$ of the $\Phi_l$ doublet (Eq. 55) is exactly as the one from an inert 2-Higgs doublet model and can be written as [114]

$$
\begin{aligned}
T=&\frac{g^2}{64\pi^2m_W^2\alpha}[F(m^2_{\phi_l^+},m_S^2)\\
&+F(m^2_{\phi_l^+},m_A^2)-F(m_S^2,m_A^2)], \qquad (58)
\end{aligned}
$$

where $m_W$ is the $W^\pm$ mass, $\alpha$ is the fine-structure constant, $g$ is the $SU(2)_L$ coupling constant and the function $F(A,B)$ is given by

$$
F(A,B)=\begin{cases}\frac{A+B}{2}-\frac{AB}{A-B}\ln\frac{A}{B}, & \text{if } A\neq B.\\ 0, & \text{if A = B.}\end{cases} \qquad (59)
$$

Although general constraints on the model are obtained, the ones that are relevant for this work are the ones with the coloured scalars running in the loops. There is a similar expression for the contribution of the coloured scalar fields to $T$ which is proportional to $F(m^2_{\phi_q^{5/3}},m^2_{\phi_q^{2/3}})$ and is given by

$$
T=\frac{3g^2}{32\pi^2m_W^2\alpha}F(m^2_{\phi_q^1},m^2_{\phi_q^2}), \qquad (60)
$$

and the most up-to-date [115] value of $T$ is $T=0.03\pm0.12$. When the masses of the coloured scalars are all taken to be equal this contribution to $T$ vanishes. However, since the masses are very large, even a small splitting could be significant. In Fig. 21 we show the value of $T$ for values of the coloured scalar mass $m_{\phi_q^1}$ of 1, 2 and 5 TeV, as a function of $\eta$ defined as $m_{\phi_q^2}=\eta\, m_{\phi_q^1}$. The experimental value of $T$ is also shown at $1\sigma$. It is clear that, contrary to the previous model where no constraints from precision oblique parameters apply, for this model and because the scalars have to be heavy, the restrictions are quite strong, forcing the masses of the two scalars to be very close. Hence, we have clearly shown the model dependence and it is also easy to understand that fields in higher isospin representations will be very con-

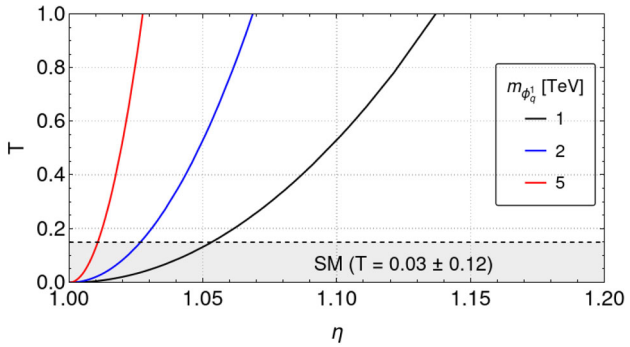


**Fig. 21** Value of the $T$ parameter for different values of the coloured scalar mass $m_{\phi_q^1}$ as a function of $\eta$ defined as $m_{\phi_q^2} = \eta\, m_{\phi_q^1}$. The experimental value of $T$ is also shown at $1\sigma$

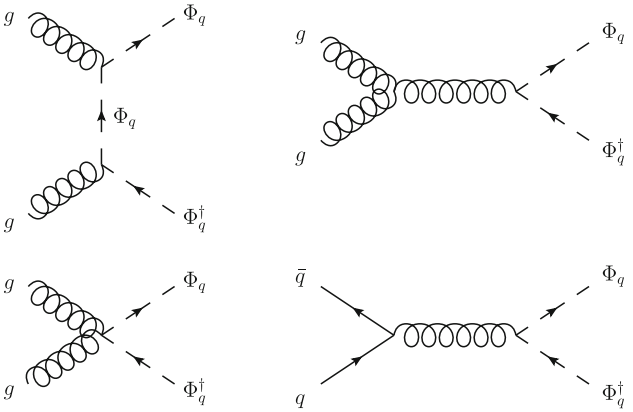


**Fig. 22** Feynman diagrams for the pair production of coloured scalar $\Phi_q$

strained in the mass splitting because of the lower limit of 1 TeV for all masses.

### 5.2 Direct searches at the LHC

We start again by noting that direct searches are model dependent. Although the production modes are controlled only by the strong coupling, the possible final states depend heavily on the model.

The generic diagrams contributing to the process $pp \to \Phi_q \Phi_q^\dagger$ is presented in Fig. 22. The cross section for $\Phi_q \Phi_q^\dagger$ production at the LHC is $\sigma(pp \to \Phi_q \Phi_q^\dagger) = 1.33 \times 10^{-1}$ fb for $m_{\Phi_q} = 1.5$ TeV and for a center of mass energy of 14 TeV. Choosing a mass of 2 TeV we obtain $\sigma(pp \to \Phi_q \Phi_q^\dagger) = 8.49 \times 10^{-3}$ fb and for a mass of 5 TeV the cross section is $\sigma(pp \to \Phi_q \Phi_q^\dagger) = 2.28 \times 10^{-9}$ fb and therefore completely negligible. Hence, already for a mass of 2 TeV the cross section is very small and we still have to decay the scalars.

The coloured scalars $\Phi_q$ do not decay directly to the DM candidate $S$. There are a number of cascade decays for $\Phi_q$ and the dominant modes for the particular case of $n = 1$ are $\Phi_q \to q\chi^\pm(q'\chi^0) \to qS\mu^\pm(q'S\nu_\mu)$ with the quarks $q$ and $q'$ representing the second- or third-generation quarks. The interactions between the SM fermions (quarks and leptons) and the new scalars arising from equation Eq. 52 exist in these model in order to introduce some lepton flavor violation, more specifically in the first and second generation. However this can be relaxed and all terms $y_{Q_i}$ and $y_{L_i}$ for the three generations can be kept non zero as long as they obey current experimental lepton flavor universality limits. For this section we only keep the second generation as an artifact of the context in which these models were proposed, connected to the muon related discrepancies. The most detectable final states at the LHC will be the following three

$$pp \to \Phi_q \Phi_q^\dagger \to (jj + \mu^+\mu^- + \not{E}_T)/(jj + \mu^\pm + \not{E}_T)/(jj + \not{E}_T), \tag{61}$$

where $j$ denotes jets in the final states. Clearly if we would study all these final states, we would cover most of the coloured scalar decays. The fact that we have muons in the final state make these two channels as more promising to be measured and probed at the LHC than the last channel in Eq. (61). Still, given the very low cross sections and the model dependence on the final states we believe that it is hard to compete with the loop induced processes even at the HL-LHC.

In order to understand the possible decay chains for the coloured scalars and to confirm whether the previous final states would cover most scalar decays, we calculate the ranges of the branching ratios with the parameters that passed all the theoretical and experimental constraints in [10] ($n = 1$) and [11] ($n = 2$). The branching ratios have been calculated with `Madgraph`'s automatic computation of decay widths, `MadWidth` [116], which includes N-body decay channels. We present in Tables 2 and 3 the maximum and minimum values for the chosen input parameters for $n = 1$ and $n = 2$, respectively. The allowed values are inside these hypercubes and were used to calculate all possible branching ratios. The detailed list of values tested can be found in Appendix C.

As discussed in the previous section, for $n = 2$, the oblique $T$ parameter forces the difference between the two coloured scalars mass to be small. In fact, we can show that for large masses the difference between the two masses must be at most around 53 GeV. Rewriting $F(m_{\phi_q^1}, m_{\phi_q^2})$ as a function of $\eta$ and expanding around $\eta = 1$ using a Taylor series we get the following form:

$$\begin{aligned} F(m_{\phi_q^1}, \eta\, m_{\phi_q^1}) &= m_{\phi_q^1}^2 \left( \frac{1+\eta^2}{2} + \frac{\eta^2}{1-\eta^2} \ln(\eta^2) \right) \\ &= m_{\phi_q^1}^2 \left( \frac{2}{3}(\eta-1)^2 + \mathcal{O}\left[(\eta-1)^4\right] \right). \end{aligned} \tag{62}$$

**Table 2** Range of the hypercube of allowed values for the model with $n = 1$. These values are the minimum and maximum allowed values for each input variable. The allowed region with all experimental and theoretical constraints is inside the hypercube

| $m_S$ | $m_A$ | $m_{\phi_q}$ | $m_\chi$ | $y_\mu$ | $y_b$ |
|---|---|---|---|---|---|
| [30,350] | [50,550] | [1000,2000] | [101,600] | [1.4,4$\pi$] | [0.25,0.65] |

Since we are considering $m_{\phi_q^1} \to \infty$ the solution will require small values of $(\eta-1)$, which means we can ignore the higher order terms. Hence, the $T$ parameter for large masses is given directly by the square of the difference between the two:

$$T = \frac{g^2}{16\pi^2 m_W^2 \alpha} \Delta M^2 \tag{63}$$

where $\Delta M = m_{\phi_q^2} - m_{\phi_q^1} = (\eta - 1)\, m_{\phi_q^1}$. Considering an upper bound of $T \leq 0.15$ at $1\sigma$ the value for $\Delta M$ for large masses is constrained by:

$$\Delta M \leq 53.1 \text{ GeV} \tag{64}$$

where we used $g^2/\alpha = 4\pi/\sin^2(\theta_W)$ and $sin^2(\theta_W) = 0.23121$ [115]. Solving instead the exact equation gives the same limit when rounded to 0.1 GeV, even for the smallest mass of $m_{\phi_q^1} = 1$ TeV, showing that this is a good approximation for the full range of masses considered. Therefore, in the direct searches study, we set $m_{\phi_q^1} = m_{\phi_q^2}$. We will discuss not only the 1.5 TeV scenario but also the ones for masses of 1.0 and 2.0 TeV with the same experimental constraints.

From Table 4 for $n = 1$, we find that the decays of all particles except the $A$ will be dominated by 2-body decays. This is due to the restrictions placed on the masses that ensure a large enough difference: $m_{\phi_q} > m_\chi + 400\,\text{GeV} > m_\chi + m_q$ and $m_\chi > m_S + 10$ GeV $> m_S + m_\mu$. The value 400 GeV comes from the restrictions imposed on the parameter space of the model and the value of 10 GeV was imposed as a minimum difference between the DM candidates. With this, the decay chain of a pair of $\phi_q$ will always start with two $\chi$ and two jets. Subsequently, the $\chi$ will most likely lead to missing energy with either one or zero muons in the final state which will produce the possibilities we presented in Eq. (61). Since we have a vectorlike fermion, the masses of $\chi^-$ and $\chi^0$ are the same and we have no decays involving $W$ bosons. However, $A$ can directly decay to $\chi$ when $m_A > m_\chi$ or alternatively to $S$ through a 3-body decay involving a virtual $\chi$ when $m_A < m_\chi$. Also, when $m_A < m_\chi$ there is the potential for a single $\chi$ to lead to 2 or 3 muons by decaying into an $A$ particle. In Table 4 we show the ranges of variation of the branching ratios (in %) for the decay of each particle and for $n = 1$ in the allowed parameter space.

For $n = 2$, the decay chain of a pair of $\phi_q$ is more difficult to study. But let us focus on the question whether the $W$ and $Z$ bosons can be important for the final products. Since the two coloured scalars have the same mass, there are no 2-body decays involving the $W$ boson. Even if we relax this condition, the oblique $T$ parameter forces the difference to be smaller then $\approx 53$ GeV ($< m_W$) for any mass values. On the other hand, the masses of $S$, $A$ and $\phi_l^+$ are generally different and, even with the oblique constraints [11], the decays with $W$ and $Z$ bosons in the final state are allowed. Thus we find large branching ratios for this type of decays (see Table 5).

When putting all the possibilities together, we conclude that if we performed three different searches, with final states of two jets and missing energy, or with at least one or at least two additional muons we would cover most of the parameter space in the different models. Therefore, if an experimental deviation relative to the SM in single and/or double Higgs production is found, a combined search of the above final states could provide some extra information. We note, however, that if we had more coloured scalars the number of final states would increase.

## 6 Conclusions

We have calculated the relative changes $\delta_h$ of SM single and $\delta_{hh}$ of SM double Higgs production when including new heavy coloured scalars. Our calculations are based on the LO cross sections at the LHC using the Fortran codes `HIGLU` and `HPAIR` where we included our new physics contributions. We have found that for an arbitrary number of scalars and taking their masses to be equal $\delta_h$ can be written as a function of only two variables, given by the sum of the couplings of the coloured particles to the Higgs boson, $\sum_i \lambda_i$, and their masses $m_i$. As for the double Higgs case, the $\delta_{hh}$ dependence extends now to three variables, the extra variable being $\sum_i \lambda_i^2$. We devised a way to find the limits on this new variable in terms of $\sum_i \lambda_i$, again for equal masses. We have discussed the limits on these variables for single Higgs production, where the results already constrain some of the parameter space. For di-Higgs production the bounds are still very loose and we have to wait until the end of Run3 to hopefully get some bounds on the couplings.

We have shown that if we relax the condition of equal masses what can be said is that the range of allowed values for $\delta_{hh}$ would be smaller than the range obtained by taking all masses equal to the smallest mass of the $n$ coloured scalars. We have also shown that taking equal couplings and performing a scan between their minimum and maximum values is sufficient to obtain the complete range for $\delta_{hh}$. In Sect. 5 we have also proven that, for a model where the coloured scalars are part of a multiplet with $n = 2$, due to the contributions to the $T$ parameter their masses are guaranteed to be similar in value with at most a 53 GeV difference. For higher values of $n$ this difference should be even more restricted. For

**Table 3** Range of the hypercube of allowed values for the model with $n = 2$. These values are the minimum and maximum allowed values for each input variable. The allowed region with all experimental and theoretical constraints is inside the hypercube

| $m_S$ | $m_A$ | $m_{\phi_l^+}$ | $m_{\phi_q^1}$ | $m_\chi$ | $y_\mu$ | $y_b$ | $\lambda_{H\Phi_l}$ |
|---|---|---|---|---|---|---|---|
| [33,76] | [45,870] | [43,619] | [1000,2000] | [101,1070] | [1.4,4$\pi$] | [0.13,0.65] | [0.025, 4$\pi$] |

**Table 4** Ranges of variation of the branching ratios (in %) for the decay of each particle and for $n = 1$ in the allowed parameter space

| $\phi_q$ | | $\chi^-$ | | $\chi^0$ | | $A$ | |
|---|---|---|---|---|---|---|---|
| $\chi^- b$ | [48.5, 53.4] | $S\ \mu^-$ | [49.9, 100] | $S\ \nu_\mu$ | [49.3, 100] | $\chi^\pm\ \mu^\mp$ | [0, 25] |
| $\chi^0 t$ | [44.1, 48.9] | $A\ \mu^-$ | [0, 49.5] | $A\ \nu_\mu$ | [0, 49.5] | $\chi^0\ \nu_\mu$ | [0, 25] |
| $\chi^- s$ | [0, 3.2] | | | | | $\mu^-\ \mu^+\ S$ | [0, 50.4] |
| $\chi^0 c$ | [0, 2.1] | | | | | $\nu_\mu\ \bar{\nu}_\mu\ S$ | [0, 50.3] |
| | | $3-Body$ | <1 | $3-Body$ | <2 | | |

**Table 5** Ranges of variation of the branching ratios (in %) for the decay of each particle and for $n = 2$ in the allowed parameter space. The last row (+2-Body) represents the remaining decays with more then two particles in the final state

| $\phi_q^{+2/3}$ | | $\phi_q^{+5/3}$ | | $\chi^-$ | |
|---|---|---|---|---|---|
| $\chi^- b$ | [0, 100] | $\chi^- t$ | [0, 100] | $S\ \mu^-$ | [25, 100] |
| $\chi^- s$ | [0, 5.9] | $\chi^- c$ | [0, 4.8] | $A\ \mu^-$ | [0, 50] |
| $\phi_l^-\ b\ \nu_\mu$ | [0, 100] | $\phi_l^-\ t\ \nu_\mu$ | [0, 51.4] | $\phi_l^-\ \nu_\mu$ | [0, 66.7] |
| $S\ b\ \mu^-$ | [0, 50.6] | $S\ t\ \mu^+$ | [0, 50.6] | | |
| $A\ b\ \mu^-$ | [0, 49.4] | $A\ t\ \mu^+$ | [0, 49.4] | | |
| +2-Body | [0, 35.7] | +2-Body | [0, 49.3] | +2-Body | [0, 6] |

| $\phi_l^+$ | | $A$ | |
|---|---|---|---|
| $S\ W^+$ | [0, 100] | $S\ Z$ | [0, 100] |
| $A\ W^+$ | [0, 49] | $\chi^\pm\ \mu^\mp$ | [0, 49.9] |
| $\chi^+\ \nu_\mu$ | [0, 99.8] | $\phi_l^\pm\ W^\mp$ | [0, 35.3] |
| $S\ \mu^+\ \nu_\mu$ | [0, 100] | $S\ \mu^-\ \mu^+$ | [0, 100] |
| $A\ \mu^+\ \nu_\mu$ | [0, 46.2] | $\phi_l^\pm\ \mu^\mp\ \nu_\mu$ | [0, 27.5] |
| +2-Body | [0, 32.4] | +2-Body | [0, 21.2] |

these models we can be confident in considering only equal masses.

Another important point to note is the complementarity between single and di-Higgs processes. Once the value of the coupling is fixed, the relative deviations from the SM move in different directions. That is, if $\delta_h$ increases $\delta_{hh}$ decreases with the coupling and vice-versa. The extra freedom of $\delta_{hh}$ also provides another venue for determining the number of scalars from observations. An excess of single or di-Higgs production could indicate the existence of $n \geq 1$ coloured scalars. But an excess of di-Higgs production paired with a single Higgs measurement close to zero would point to $n > 1$.

One final and very important point to note is that in direct searches for DM at the LHC we do not have access to the number of DM fields because we only look for missing energy associated with some SM particle in the final state. On the contrary, in our approach the number of fields is a variable that influences the results.

**Acknowledgements** PG is supported by the Portuguese Foundation for Science and Technology (FCT) with a PhD Grant no. 2022.11377. BD. PG, DN and RS are partially supported by FCT under Contracts no. UIDB/00618/2020, UIDP/00618/2020, PTDC/FIS-PAR/31000/2017 and CERN/FIS-PAR/0014 /2019. The work of MM is supported by the DFG Collaborative Research Center TRR257 "Particle Physics Phenomenology after the Higgs Discovery".

**Data Availibility Statement** This manuscript has no associated data. [Author's comment: Data sharing not applicable to this article as no datasets were generated or analysed during the current study.]

**Code Availibility Statement** This manuscript has associated code/-software in a data repository. [Author's comment: The code/software generated during and/or analysed during the current study is available in the HPAIR-SCALARS repository, https://gitlab.com/bdm-models/higgs-production/hpair-scalars (Ref. [117]).]

Funded by SCOAP[3].

## Appendix A: HPAIR extension to coloured scalars

In the following we present our implementation of the contributions from the coloured scalars to Higgs pair production at leading order in the code HPAIR. It has been made available at [117]. All changes of the original source code are contained entirely within hpair.f. The code is compiled by using make and then running the executable run which will assume the input and output files hpair.**in** and hpair.**out** respectively. For the compilation process the LHAPDF libraries required by HPAIR must be supplied and their installation path indicated with the variable LIBS in the makefile.

The new input options are contained within the original input file of HPAIR, hpair.**in**. The following lines delimit where these new options are found:

```
!------------------------------------------------
!SCALARS LOOP OPTIONS:
!================
(...)
!---------------------- SCALARS LOOP OPTIONS END ----
```

By setting the variable iscalars to 1, the coloured scalar form factors are added to the SM amplitude. The type of model, characterised by the number of scalars $n$, is selected with the variable iNscalars. These are found in the following block:

```
!IF iscalars=1 THEN THE NEW SCALARS DIAGRAMS WILL BE
    ADDED TO F1
iscalars = 1
!SELECT NUMBER OF SCALARS: for n >= 2 all masses and
    couplings are considered equal
iNscalars= 1
```

When iNscalars is set to either 1 or 2, this corresponds to a model with 1 or 2 scalars, respectively. For each model type the masses in GeV, mphiq, and couplings to the Higgs, lambHPQ, must be supplied. These input parameters are set in the following blocks:

```
!MODEL (n=1) PARAMETERS:
mphiq1    = 2000.D0
lambHPQ1 = 1.0D0

!MODEL (n=2) PARAMETERS:
mphiq1    = 1000.D0
mphiq2    = 1000.D0
lambHPQ1 = 1.000D0
lambHPQ2 = 1.000D0
```

On the other hand, setting iNscalars to >= 2 comes with the limitation that all the scalars must have the same mass, mphiq1, and coupling, lambHPQ1. These 2 input parameters can be set in the following block:

```
!MODEL (n>=2) PARAMETERS:
mphiq1    = 1200.D0
lambHPQ1 = 12.D0
```

The final block of parameters relates to the individual form factor selection and it applies to all scalars. The relevant lines are:

```
!DIAGRAMS/FORM FACTORS SELECTION:
!IF FULL=1 THEN FULL FORMULA IS USED INSTEAD
full      = 1
triang    = 1
boxTri    = 1
boxQuad   = 0
```

The variable full is used to select whether all the NP form factors, as presented in Eqs. (30) and (32), are automatically included in the amplitude ( full =1) or not ( full =0). In the latter case, the following three variables triang, boxTri and boxQuad are used to determine which form factors are to be included in the calculations:

- triang =1: Will include the triangle form factor $g^h_{\phi_q} F^{\phi_q}_{\triangle}$ (Eq. (5)) originating from the triangle diagrams (Fig. 8b, c)
- boxTri =1: Will include the box form factors $(g^h_{\phi_q})^2 G^{\phi_q}_{\square_1}$ and $(g^h_{\phi_q})^2 F^{\phi_q}_{\square_1}$ (Eqs. (34, 35)) originating from the box diagrams with the triple couplings between one Higgs and two coloured scalars (Fig. 9b, c)
- boxQuad =1: Will include the box form factor $(g^{hh}_{\phi_q}) F^{\phi_q}_{\square_2}$ (Eq. (5), as $F^{\phi_q}_{\square_2} = F^{\phi_q}_{\triangle}$) originating from the box diagrams with the quartic couplings between two Higgs and two coloured scalars (Fig. 9d, e)

Some care in the formatting must be taken when changing the values of the parameters. The code uses the number of the lines to identify the input parameters and thus they must be preserved. The names of the variables indicated in the input file have no impact. However, the number of characters before the equal sign must always be nine in total:

```
mphiq1___= 1
9 charaters
```

These considerations are important to keep in mind when using a script to automatically change the input values.

The output file suffers no changes from the original HPAIR template, hpair.**out**. The NP contributions only affect

the LO cross section which can be extracted from the following line:

```
SIGMA_BORN = (  2.0478260337291408E-002  +-
     2.4261364431116920E-005 ) PB
```

where the Mandelstam variables $s, t, u$ are defined as:

$$s = (p_a + p_b)^2 \quad t = (p_a - p_c)^2 \quad u = (p_b - p_c)^2. \tag{67}$$

They also involve the following scalar integrals:

$$C_{ab} = \int \frac{d^4q}{i\pi^2} \frac{1}{\left(q^2 - m_X^2\right)\left((q+p_a)^2 - m_X^2\right)\left((q+p_a+p_b)^2 - m_X^2\right)} \tag{68}$$

$$D_{abc} = \int \frac{d^4q}{i\pi^2} \frac{1}{\left(q^2 - m_X^2\right)\left((q+p_a)^2 - m_X^2\right)\left((q+p_a+p_b)^2 - m_X^2\right)\left((q+p_a+p_b+p_c)^2 - m_X^2\right)} \tag{69}$$

## Appendix B: Double Higgs production

For completeness, we repeat here the SM box form factors appearing in Eq. (32), which can also be found e.g. in [77]. They are given by:

$$\begin{aligned}
F_{\square}^{Q} = \frac{2m_Q^2}{s}\Bigg(& 2 + (4m_Q^2)C_{ab}^{m_Q^2} \\
&+\frac{2}{s}(t - m_h^2)(m_h^2 - 4m_Q^2)C_{ac}^{m_Q^2} \\
&+\frac{2}{s}(u - m_h^2)(m_h^2 - 4m_Q^2)C_{bc}^{m_Q^2} \\
&-m_Q^2(s + 2m_h^2 - 8m_Q^2)(D_{abc}^{m_Q^2} + D_{bac}^{m_Q^2}) \\
&+(m_Q^2(s + 2m_h^2 - 8m_Q^2) \\
&-\frac{1}{s}(m_h^2 - 4m_Q^2)(tu - m_h^4))D_{acb}^{m_Q^2}\Bigg)
\end{aligned} \tag{65}$$

$$\begin{aligned}
G_{\square}^{Q} = \frac{2m_Q^2}{s}& \left(\frac{1}{tu - m_h^4}\right) \\
&\times\Bigg(\frac{s}{2}(t^2 + u^2 + 2m_h^4 - 8m_Q^2(t+u))C_{ab}^{m_Q^2} \\
&+(t^2 + m_h^4 - 8tm_Q^2)(t - m_h^2)C_{ac}^{m_Q^2} \\
&+(u^2 + m_h^4 - 8um_Q^2)(u - m_h^2)C_{bc}^{m_Q^2} \\
&-\frac{1}{2}(t^2 + u^2 - 2m_h^4)(t + u - 8m_Q^2)C_{cd}^{m_Q^2} \\
&-(st(t^2/2 + m_h^4/2 - 4tm_Q^2) \\
&+m_Q^2(t + u - 8m_Q^2)(tu - m_h^4))D_{bac}^{m_Q^2} \\
&-(su(u^2/2 + m_h^4/2 - 4um_Q^2) \\
&+m_Q^2(t + u - 8m_Q^2)(tu - m_h^4))D_{abc}^{m_Q^2} \\
&-m_Q^2(t + u - 8m_Q^2)(tu - m_h^4)D_{acb}^{m_Q^2}\Bigg)
\end{aligned} \tag{66}$$

where $X$ stands for the quark or coloured scalar as appropriate. The exact formula for $C_{ab}$ has been determined and is given by:

$$C_{ab} = -\frac{2}{s} f(\tau) \tag{70}$$

where $f_\tau$ is given in Eq. (6) and $\tau = \frac{4m_X^2}{s}$.

## Appendix C: Parameters tested for the branching ratios

Below we present the values of the parameters used in determining the branching ratios with `MadWidth` [116]. They were chosen as to comply with the theoretical and experimental constraints in [10] ($n = 1$) and [11] ($n = 2$) (Tables 6, 7, 8, 9, 10).

**Table 6** Model 5 (n = 1): all particles decays were calculated for all the combinations of masses presented above. For the Yukawa couplings we only calculated the decays with either both parameters at their minimum values ($y_b = 0.25,\ y_\mu = 1.4$) or both parameters at their maximum values ($y_b = 0.65,\ y_\mu = 3.55$)

| | |
|---|---|
| $m_S$ | 30 60 90 120 150 200 250 300 350 |
| $m_A$ | 50 150 250 350 450 550 |
| $m_\chi$ | 100 200 300 400 500 600 |
| $m_{\phi_q^{2/5}}$ | 1000 |
| $(y_b, y_\mu)$ | (0.25, 1.4) (0.65, 3.55) |

**Table 7** Model 3 (n = 2): parameters tested for the $A$ decays

| | |
|---|---|
| $m_S$ | 33 40 50 60 76 |
| $m_A$ | 43 50 75 100 200 400 600 870 |
| $m_{\phi_l^+}$ | 43 50 100 200 400 500 619 |
| $m_\chi$ | 100 150 300 500 700 1070 |
| $m_{\phi_q^1} = m_{\phi_q^2}$ | 1000 |
| $y_b$ | 0.15 0.65 |
| $y_\mu$ | 12 |

**Table 8** Model 3 (n = 2): parameters tested for the $\phi_l$ decays

| | |
|---|---|
| $m_S$ | 33 50 76 |
| $m_A$ | 43 400 870 |
| $m_{\phi_l^+}$ | 45 60 100 200 300 400 450 500 550 600 |
| $m_\chi$ | 100 300 500 800 1000 |
| $m_{\phi_q^1} = m_{\phi_q^2}$ | 1000 |
| $y_b$ | 0.15 0.65 |
| $y_\mu$ | 2 5 9 12 |

**Table 9** Model 3 (n = 2): parameters tested for the $\chi$ decays

| | |
|---|---|
| $m_S$ | 76 |
| $m_A$ | 86 100 250 450 650 870 |
| $m_{\phi_l^+}$ | 86 100 200 400 500 619 |
| $m_\chi$ | 100 200 300 400 500 600 700 800 900 1000 |
| $m_{\phi_q^1} = m_{\phi_q^2}$ | 1000 |
| $y_b$ | 0.15 0.65 |
| $y_\mu$ | 12 |

**Table 10** Model 3 (n = 2): parameters tested for the $\phi_q^1$ or $\phi_q^2$ decays

| | |
|---|---|
| $m_S$ | 40 |
| $m_A$ | 100 |
| $m_{\phi_l^+}$ | 45 180 300 600 |
| $m_\chi$ | 100 200 300 400 500 600 700 800 900 1000 |
| $m_{\phi_q^1} = m_{\phi_q^2}$ | 1000 1500 2000 |
| $y_b$ | 0.15 0.35 0.65 |
| $y_\mu$ | 2 8 12 |

## References


1. LHCb Collaboration, R. Aaij et al., Test of lepton universality in beauty-quark decays. Nat. Phys. **18**, 277–282 (2022). https://doi.org/10.1038/s41567-021-01478-8. arXiv:2103.11769
2. LHCb Collaboration, R. Aaij et al., Search for lepton-universality violation in $B^+ \to K^+\ell^+\ell^-$ decays. Phys. Rev. Lett. **122**, 191801 (2019). https://doi.org/10.1103/PhysRevLett.122.191801. arXiv:1903.09252
3. Muon g-2 Collaboration, D.P. Aguillard et al., Measurement of the positive muon anomalous magnetic moment to 0.20 ppm. arXiv:2308.06230
4. Particle Data Group Collaboration, M. Tanabashi et al., Review of particle physics. Phys. Rev. D **98**, 030001 (2018). https://doi.org/10.1103/PhysRevD.98.030001
5. T.P. Gorringe, D.W. Hertzog, Precision muon physics. Prog. Part. Nucl. Phys. **84**, 73–123 (2015). https://doi.org/10.1016/j.ppnp.2015.06.001. arXiv:1506.01465
6. T. Aoyama et al., The anomalous magnetic moment of the muon in the Standard Model. Phys. Rep. **887**, 1–166 (2020). https://doi.org/10.1016/j.physrep.2020.07.006. arXiv:2006.04822
7. Muon g-2 Collaboration, G.W. Bennett et al., Final report of the muon E821 anomalous magnetic moment measurement at BNL. Phys. Rev. D **73**, 072003 (2006). https://doi.org/10.1103/PhysRevD.73.072003. arXiv:hep-ex/0602035
8. LHCb Collaboration, Measurement of lepton universality parameters in $B^+ \to K^+\ell^+\ell^-$ and $B^0 \to K^{*0}\ell^+\ell^-$ decays. arXiv:2212.09153
9. LHCb Collaboration, Test of lepton universality in $b \to s\ell^+\ell^-$ decays. arXiv:2212.09152
10. D. Huang, A.P. Morais, R. Santos, Anomalies in $B$-meson decays and the muon $g-2$ from dark loops. Phys. Rev. D **102**, 075009 (2020). https://doi.org/10.1103/PhysRevD.102.075009. arXiv:2007.05082
11. R. Capucha, D. Huang, T. Lopes, R. Santos, Impact of electroweak group representation in models for B and g-2 anomalies from dark loops. Phys. Rev. D **106**, 095032 (2022). https://doi.org/10.1103/PhysRevD.106.095032. arXiv:2207.11556
12. D.G. Cerdeño, A. Cheek, P. Martín-Ramiro, J.M. Moreno, B anomalies and dark matter: a complex connection. Eur. Phys. J. C **79**, 517 (2019). https://doi.org/10.1140/epjc/s10052-019-6979-x. arXiv:1902.01789
13. ATLAS Collaboration, M. Aaboud et al., Search for dark matter produced in association with bottom or top quarks in $\sqrt{s} = 13$ TeV pp collisions with the ATLAS detector. Eur. Phys. J. C **78**, 18 (2018). https://doi.org/10.1140/epjc/s10052-017-5486-1. arXiv:1710.11412
14. H.M. Georgi, S.L. Glashow, M.E. Machacek, D.V. Nanopoulos, Higgs bosons from two gluon annihilation in proton proton collisions. Phys. Rev. Lett. **40**, 692 (1978). https://doi.org/10.1103/PhysRevLett.40.692
15. M. Spira, Higgs boson production and decay at hadron colliders. Prog. Part. Nucl. Phys. **95**, 98–159 (2017). https://doi.org/10.1016/j.ppnp.2017.04.001. arXiv:1612.07651
16. M. Spira, HIGLU: a program for the calculation of the total Higgs production cross-section at hadron colliders via gluon fusion including QCD corrections. arXiv:hep-ph/9510347
17. A. Djouadi, M. Spira, P. Zerwas, Production of Higgs bosons in proton colliders. QCD corrections. Phys. Lett. B **264**, 440–446 (1991). https://doi.org/10.1016/0370-2693(91)90375-Z
18. S. Dawson, Radiative corrections to Higgs boson production. Nucl. Phys. B **359**, 283–300 (1991). https://doi.org/10.1016/0550-3213(91)90061-2
19. D. Graudenz, M. Spira, P.M. Zerwas, QCD corrections to Higgs boson production at proton proton colliders. Phys. Rev. Lett. **70**, 1372–1375 (1993). https://doi.org/10.1103/PhysRevLett.70.1372
20. M. Spira, A. Djouadi, D. Graudenz, P.M. Zerwas, Higgs boson production at the LHC. Nucl. Phys. B **453**, 17–82 (1995). https://doi.org/10.1016/0550-3213(95)00379-7. arXiv:hep-ph/9504378
21. R. Harlander, P. Kant, Higgs production and decay: analytic results at next-to-leading order QCD. JHEP **12**, 015 (2005). https://doi.org/10.1088/1126-6708/2005/12/015. arXiv:hep-ph/0509189
22. C. Anastasiou, S. Beerli, S. Bucherer, A. Daleo, Z. Kunszt, Two-loop amplitudes and master integrals for the production of a Higgs boson via a massive quark and a scalar-quark loop. JHEP **01**, 082 (2007). https://doi.org/10.1088/1126-6708/2007/01/082. arXiv:hep-ph/0611236
23. U. Aglietti, R. Bonciani, G. Degrassi, A. Vicini, Analytic results for virtual QCD corrections to Higgs production and decay. JHEP **01**, 021 (2007). https://doi.org/10.1088/1126-6708/2007/01/021. arXiv:hep-ph/0611266
24. C. Anastasiou, S. Bucherer, Z. Kunszt, HPro: a NLO Monte-Carlo for Higgs production via gluon fusion with finite heavy quark masses. JHEP **10**, 068 (2009). https://doi.org/10.1088/1126-6708/2009/10/068. arXiv:0907.2362
25. S. Catani, D. de Florian, M. Grazzini, Higgs production in hadron collisions: soft and virtual QCD corrections at NNLO. JHEP **05**, 025 (2001). https://doi.org/10.1088/1126-6708/2001/05/025. arXiv:hep-ph/0102227

26. R.V. Harlander, W.B. Kilgore, Soft and virtual corrections to proton proton –> H + x at NNLO. Phys. Rev. D **64**, 013015 (2001). https://doi.org/10.1103/PhysRevD.64.013015. arXiv:hep-ph/0102241
27. R.V. Harlander, W.B. Kilgore, Next-to-next-to-leading order Higgs production at hadron colliders. Phys. Rev. Lett. **88**, 201801 (2002). https://doi.org/10.1103/PhysRevLett.88.201801. arXiv:hep-ph/0201206
28. C. Anastasiou, K. Melnikov, Higgs boson production at hadron colliders in NNLO QCD. Nucl. Phys. B **646**, 220–256 (2002). https://doi.org/10.1016/S0550-3213(02)00837-4. arXiv:hep-ph/0207004
29. V. Ravindran, J. Smith, W. van Neerven, NNLO corrections to the total cross section for Higgs boson production in hadron-hadron collisions. Nucl. Phys. B **665**, 325–366 (2003). https://doi.org/10.1016/S0550-3213(03)00457-7
30. S. Marzani, R.D. Ball, V. Del Duca, S. Forte, A. Vicini, Higgs production via gluon–gluon fusion with finite top mass beyond next-to-leading order. Nucl. Phys. B **800**, 127–145 (2008). https://doi.org/10.1016/j.nuclphysb.2008.03.016
31. T. Gehrmann, M. Jaquier, E.W.N. Glover, A. Koukoutsakis, Two-Loop QCD corrections to the helicity amplitudes for $H \to 3$ partons. JHEP **02**, 056 (2012). https://doi.org/10.1007/JHEP02(2012)056. arXiv:1112.3554
32. C. Anastasiou, C. Duhr, F. Dulat, B. Mistlberger, Soft triple-real radiation for Higgs production at N3LO. JHEP **07**, 003 (2013). https://doi.org/10.1007/JHEP07(2013)003. arXiv:1302.4379
33. C. Anastasiou, C. Duhr, F. Dulat, F. Herzog, B. Mistlberger, Real-virtual contributions to the inclusive Higgs cross-section at $N^3LO$. JHEP **12**, 088 (2013). https://doi.org/10.1007/JHEP12(2013)088. arXiv:1311.1425
34. W.B. Kilgore, One-loop single-real-emission contributions to $pp \to H + X$ at next-to-next-to-next-to-leading order. Phys. Rev. D **89**, 073008 (2014). https://doi.org/10.1103/PhysRevD.89.073008. arXiv:1312.1296
35. Y. Li, A. von Manteuffel, R.M. Schabinger, H.X. Zhu, $N^3LO$ Higgs boson and Drell–Yan production at threshold: the one-loop two-emission contribution. Phys. Rev. D **90**, 053006 (2014). https://doi.org/10.1103/PhysRevD.90.053006. arXiv:1404.5839
36. C. Anastasiou, C. Duhr, F. Dulat, E. Furlan, T. Gehrmann, F. Herzog et al., Higgs boson gluon fusion production beyond threshold in $N^3LO$ QCD. JHEP **03**, 091 (2015). https://doi.org/10.1007/JHEP03(2015)091. arXiv:1411.3584
37. C. Anastasiou, C. Duhr, F. Dulat, F. Herzog, B. Mistlberger, Higgs boson gluon-fusion production in QCD at three loops. Phys. Rev. Lett. **114**, 212001 (2015). https://doi.org/10.1103/PhysRevLett.114.212001. arXiv:1503.06056
38. C. Anastasiou, C. Duhr, F. Dulat, E. Furlan, T. Gehrmann, F. Herzog et al., High precision determination of the gluon fusion Higgs boson cross-section at the LHC. JHEP **05**, 058 (2016). https://doi.org/10.1007/JHEP05(2016)058. arXiv:1602.00695
39. B. Mistlberger, Higgs boson production at hadron colliders at $N^3LO$ in QCD. JHEP **05**, 028 (2018). https://doi.org/10.1007/JHEP05(2018)028. arXiv:1802.00833
40. C. Duhr, B. Mistlberger, G. Vita, Soft integrals and soft anomalous dimensions at $N^3LO$ and beyond. JHEP **09**, 155 (2022). https://doi.org/10.1007/JHEP09(2022)155. arXiv:2205.04493
41. J. Baglio, C. Duhr, B. Mistlberger, R. Szafron, Inclusive production cross sections at $N^3LO$. JHEP **12**, 066 (2022). https://doi.org/10.1007/JHEP12(2022)066. arXiv:2209.06138
42. R.V. Harlander, K.J. Ozeren, Top mass effects in Higgs production at next-to-next-to-leading order QCD: virtual corrections. Phys. Lett. B **679**, 467–472 (2009). https://doi.org/10.1016/j.physletb.2009.08.012. arXiv:0907.2997
43. R.V. Harlander, K.J. Ozeren, Finite top mass effects for hadronic Higgs production at next-to-next-to-leading order. JHEP **11**, 088 (2009). https://doi.org/10.1088/1126-6708/2009/11/088. arXiv:0909.3420
44. R.V. Harlander, H. Mantler, S. Marzani, K.J. Ozeren, Higgs production in gluon fusion at next-to-next-to-leading order QCD for finite top mass. Eur. Phys. J. C **66**, 359–372 (2010). https://doi.org/10.1140/epjc/s10052-010-1258-x. arXiv:0912.2104
45. A. Pak, M. Rogal, M. Steinhauser, Finite top quark mass effects in NNLO Higgs boson production at LHC. JHEP **02**, 025 (2010). https://doi.org/10.1007/JHEP02(2010)025. arXiv:0911.4662
46. C. Anastasiou, N. Deutschmann, A. Schweitzer, Quark mass effects in two-loop Higgs amplitudes. JHEP **07**, 113 (2020). https://doi.org/10.1007/JHEP07(2020)113. arXiv:2001.06295
47. M.L. Czakon, M. Niggetiedt, Exact quark-mass dependence of the Higgs-gluon form factor at three loops in QCD. JHEP **05**, 149 (2020). https://doi.org/10.1007/JHEP05(2020)149. arXiv:2001.03008
48. M. Niggetiedt, J. Usovitsch, The Higgs-gluon form factor at three loops in QCD with three mass scales. JHEP **02**, 087 (2024). https://doi.org/10.1007/JHEP02(2024)087. arXiv:2312.05297
49. R. Bonciani, G. Degrassi, A. Vicini, Scalar particle contribution to Higgs production via gluon fusion at NLO. JHEP **11**, 095 (2007). https://doi.org/10.1088/1126-6708/2007/11/095. arXiv:0709.4227
50. R. Boughezal, F. Petriello, Color-octet scalar effects on Higgs boson production in gluon fusion. Phys. Rev. D **81**, 114033 (2010). https://doi.org/10.1103/PhysRevD.81.114033. arXiv:1003.2046
51. R. Boughezal, Constraints on heavy colored scalars from Tevatron's Higgs exclusion limit. Phys. Rev. D **83**, 093003 (2011). https://doi.org/10.1103/PhysRevD.83.093003. arXiv:1101.3769
52. M. Muhlleitner, M. Spira, Higgs boson production via gluon fusion: squark loops at NLO QCD. Nucl. Phys. B **790**, 1–27 (2008). https://doi.org/10.1016/j.nuclphysb.2007.08.011. arXiv:hep-ph/0612254
53. R.V. Harlander, M. Steinhauser, Supersymmetric Higgs production in gluon fusion at next-to-leading order. JHEP **09**, 066 (2004). https://doi.org/10.1088/1126-6708/2004/09/066. arXiv:hep-ph/0409010
54. R.V. Harlander, M. Steinhauser, Hadronic Higgs production and decay in supersymmetry at next-to-leading order. Phys. Lett. B **574**, 258–268 (2003). https://doi.org/10.1016/j.physletb.2003.09.013. arXiv:hep-ph/0307346
55. R.V. Harlander, F. Hofmann, H. Mantler, Supersymmetric Higgs production in gluon fusion. JHEP **02**, 055 (2011). https://doi.org/10.1007/JHEP02(2011)055. arXiv:1012.3361
56. G. Degrassi, P. Slavich, On the NLO QCD corrections to Higgs production and decay in the MSSM. Nucl. Phys. B **805**, 267–286 (2008). https://doi.org/10.1016/j.nuclphysb.2008.07.022. arXiv:0806.1495
57. G. Degrassi, P. Slavich, NLO QCD bottom corrections to Higgs boson production in the MSSM. JHEP **11**, 044 (2010). https://doi.org/10.1007/JHEP11(2010)044. arXiv:1007.3465
58. R. Harlander, M. Steinhauser, Effects of SUSY QCD in hadronic Higgs production at next-to-next-to-leading order. Phys. Rev. D **68**, 111701 (2003). https://doi.org/10.1103/PhysRevD.68.111701. arXiv:hep-ph/0308210
59. A. Belyaev, M. Drees, O.J.P. Eboli, J.K. Mizukoshi, S.F. Novaes, Supersymmetric Higgs pair production at hadron colliders. Phys. Rev. D **60**, 075008 (1999). https://doi.org/10.1103/PhysRevD.60.075008. arXiv:hep-ph/9905266
60. A. Djouadi, P. Gambino, Leading electroweak correction to Higgs boson production at proton colliders. Phys. Rev. Lett. **73**, 2528–2531 (1994). https://doi.org/10.1103/PhysRevLett.73.2528. arXiv:hep-ph/9406432
61. K.G. Chetyrkin, B.A. Kniehl, M. Steinhauser, Three loop O (alpha-s**2 G(F) M(t)**2) corrections to hadronic Higgs

decays. Nucl. Phys. B **490**, 19–39 (1997). https://doi.org/10.1016/S0550-3213(97)00051-5. arXiv:hep-ph/9701277
62. K.G. Chetyrkin, B.A. Kniehl, M. Steinhauser, Virtual top quark effects on the H –> b anti-b decay at next-to-leading order in QCD. Phys. Rev. Lett. **78**, 594–597 (1997). https://doi.org/10.1103/PhysRevLett.78.594. arXiv:hep-ph/9610456
63. G. Degrassi, F. Maltoni, Two-loop electroweak corrections to Higgs production at hadron colliders. Phys. Lett. B **600**, 255–260 (2004). https://doi.org/10.1016/j.physletb.2004.09.008. arXiv:hep-ph/0407249
64. U. Aglietti, R. Bonciani, G. Degrassi, A. Vicini, Two-loop electroweak corrections to Higgs production in proton–proton collisions, in *TeV4LHC Workshop: 2nd Meeting, 10* (2006). arXiv:hep-ph/0610033
65. S. Actis, G. Passarino, C. Sturm, S. Uccirati, NLO electroweak corrections to Higgs boson production at hadron colliders. Phys. Lett. B **670**, 12–17 (2008). https://doi.org/10.1016/j.physletb.2008.10.018. arXiv:0809.1301
66. S. Actis, G. Passarino, C. Sturm, S. Uccirati, NNLO computational techniques: the cases H –> gamma gamma and H –> g g. Nucl. Phys. B **811**, 182–273 (2009). https://doi.org/10.1016/j.nuclphysb.2008.11.024. arXiv:0809.3667
67. C. Anastasiou, R. Boughezal, F. Petriello, Mixed QCD-electroweak corrections to Higgs boson production in gluon fusion. JHEP **04**, 003 (2009). https://doi.org/10.1088/1126-6708/2009/04/003. arXiv:0811.3458
68. J. Butterworth et al., PDF4LHC recommendations for LHC Run II. J. Phys. G **43**, 023001 (2016). https://doi.org/10.1088/0954-3899/43/2/023001. arXiv:1510.03865
69. NNPDF Collaboration, R.D. Ball et al., The path to proton structure at 1% accuracy. Eur. Phys. J. C **82**, 428 (2022). https://doi.org/10.1140/epjc/s10052-022-10328-7. arXiv:2109.02653
70. A. Crivellin, L. Schnell, Complete Lagrangian and set of Feynman rules for scalar leptoquarks. Comput. Phys. Commun. **271**, 108188 (2022). https://doi.org/10.1016/j.cpc.2021.108188. arXiv:2105.04844
71. P.M. Ferreira, R. Santos, A. Barroso, Stability of the tree-level vacuum in two Higgs doublet models against charge or CP spontaneous violation. Phys. Lett. B **603**, 219–229 (2004). https://doi.org/10.1016/j.physletb.2004.10.022. arXiv:hep-ph/0406231
72. ATLAS Collaboration, G. Aad et al., Combined measurements of Higgs boson production and decay using up to 80 $\text{fb}^{-1}$ of proton–proton collision data at $\sqrt{s} = 13$ TeV collected with the ATLAS experiment. Phys. Rev. D **101**, 012002 (2020). https://doi.org/10.1103/PhysRevD.101.012002. arXiv:1909.02845
73. CMS Collaboration, A.M. Sirunyan et al., Combined measurements of Higgs boson couplings in proton–proton collisions at $\sqrt{s} = 13$ TeV. Eur. Phys. J. C **79**, 421 (2019). https://doi.org/10.1140/epjc/s10052-019-6909-y. arXiv:1809.10733
74. M. Cepeda, S. Gori, P. Ilten, M. Kado, F. Riva, R.A. Khalek et al., Higgs physics at the HL-LHC and HE-LHC. arXiv:1902.00134
75. LHC Higgs Cross Section Working Group Collaboration, D. de Florian et al., Handbook of LHC Higgs cross sections: 4. deciphering the nature of the Higgs Sector. arXiv:1610.07922
76. E.W.N. Glover, J.J. van der Bij, Higgs boson pair production via gluon fusion. Nucl. Phys. B **309**, 282–294 (1988). https://doi.org/10.1016/0550-3213(88)90083-1
77. T. Plehn, M. Spira, P.M. Zerwas, Pair production of neutral Higgs particles in gluon–gluon collisions. Nucl. Phys. B **479**, 46–64 (1996). https://doi.org/10.1016/0550-3213(96)00418-X. arXiv:hep-ph/9603205
78. T. Hahn, Generating Feynman diagrams and amplitudes with FeynArts 3. Comput. Phys. Commun. **40**, 418–431 (2001). https://doi.org/10.1016/S0010-4655(01)00290-9
79. T. Hahn, FeynArts 3.11 user's guide. https://feynarts.de/FA3Guide.pdf. Accessed 26 July 2023
80. G.D. Kribs, A. Martin, Enhanced di-Higgs production through light colored scalars. Phys. Rev. D **86**, 095023 (2012). https://doi.org/10.1103/PhysRevD.86.095023. arXiv:1207.4496
81. T. Enkhbat, Scalar leptoquarks and Higgs pair production at the LHC. JHEP **01**, 158 (2014). https://doi.org/10.1007/JHEP01(2014)158. arXiv:1311.4445
82. S. Dawson, S. Dittmaier, M. Spira, Neutral Higgs boson pair production at hadron colliders: QCD corrections. Phys. Rev. D **58**, 115012 (1998). https://doi.org/10.1103/PhysRevD.58.115012. arXiv:hep-ph/9805244
83. S. Borowka, N. Greiner, G. Heinrich, S.P. Jones, M. Kerner, J. Schlenk et al., Higgs boson pair production in gluon fusion at next-to-leading order with full top-quark mass dependence. Phys. Rev. Lett. **117**, 012001 (2016). https://doi.org/10.1103/PhysRevLett.117.079901. arXiv:1604.06447
84. S. Borowka, N. Greiner, G. Heinrich, S.P. Jones, M. Kerner, J. Schlenk et al., Full top quark mass dependence in Higgs boson pair production at NLO. JHEP **10**, 107 (2016). https://doi.org/10.1007/JHEP10(2016)107. arXiv:1608.04798
85. J. Baglio, F. Campanario, S. Glaus, M. MÃŒhlleitner, M. Spira, J. Streicher, Gluon fusion into Higgs pairs at NLO QCD and the top mass scheme. Eur. Phys. J. C **79**, 459 (2019). https://doi.org/10.1140/epjc/s10052-019-6973-3. arXiv:1811.05692
86. J. Baglio, F. Campanario, S. Glaus, M. Mühlleitner, J. Ronca, M. Spira et al., Higgs-pair production via gluon fusion at hadron colliders: NLO QCD corrections. JHEP **04**, 181 (2020). https://doi.org/10.1007/JHEP04(2020)181. arXiv:2003.03227
87. J. Baglio, F. Campanario, S. Glaus, M. Mühlleitner, J. Ronca, M. Spira, $gg \to HH$: combined uncertainties. Phys. Rev. D **103**, 056002 (2021). https://doi.org/10.1103/PhysRevD.103.056002. arXiv:2008.11626
88. D. de Florian, J. Mazzitelli, Higgs boson pair production at next-to-next-to-leading order in QCD. Phys. Rev. Lett. **111**, 201801 (2013). https://doi.org/10.1103/PhysRevLett.111.201801. arXiv:1309.6594
89. J. Grigo, K. Melnikov, M. Steinhauser, Virtual corrections to Higgs boson pair production in the large top quark mass limit. Nucl. Phys. B **888**, 17–29 (2014). https://doi.org/10.1016/j.nuclphysb.2014.09.003. arXiv:1408.2422
90. D.Y. Shao, C.S. Li, H.T. Li, J. Wang, Threshold resummation effects in Higgs boson pair production at the LHC. JHEP **07**, 169 (2013). https://doi.org/10.1007/JHEP07(2013)169. arXiv:1301.1245
91. D. de Florian, J. Mazzitelli, Higgs pair production at next-to-next-to-leading logarithmic accuracy at the LHC. JHEP **09**, 053 (2015). https://doi.org/10.1007/JHEP09(2015)053. arXiv:1505.07122
92. P. Banerjee, S. Borowka, P.K. Dhani, T. Gehrmann, V. Ravindran, Two-loop massless QCD corrections to the $g + g \to H + H$ four-point amplitude. JHEP **11**, 130 (2018). https://doi.org/10.1007/JHEP11(2018)130. arXiv:1809.05388
93. L.-B. Chen, H.T. Li, H.-S. Shao, J. Wang, Higgs boson pair production via gluon fusion at $\text{N}^3\text{LO}$ in QCD. Phys. Lett. B **803**, 135292 (2020). https://doi.org/10.1016/j.physletb.2020.135292. arXiv:1909.06808
94. L.-B. Chen, H.T. Li, H.-S. Shao, J. Wang, The gluon-fusion production of Higgs boson pair: $\text{N}^3\text{LO}$ QCD corrections and top-quark mass effects. JHEP **03**, 072 (2020). https://doi.org/10.1007/JHEP03(2020)072. arXiv:1912.13001
95. A.H. Ajjath, H.-S. Shao, $\text{N}^3\text{LO+N}^3\text{LL}$ QCD improved Higgs pair cross sections. JHEP **02**, 067 (2023). https://doi.org/10.1007/JHEP02(2023)067. arXiv:2209.03914
96. J. Alison et al., Higgs boson potential at colliders: status and perspectives. Rev. Phys. **5**, 100045 (2020). https://doi.org/10.1016/j.revip.2020.100045. arXiv:1910.00012
97. A. Agostini, G. Degrassi, R. Gröber, P. Slavich, NLO-QCD corrections to Higgs pair production in the MSSM.

JHEP **04**, 106 (2016). https://doi.org/10.1007/JHEP04(2016)106. arXiv:1601.03671
98. P. Huang, A. Joglekar, M. Li, C.E.M. Wagner, Corrections to di-Higgs boson production with light stops and modified Higgs couplings. Phys. Rev. D **97**, 075001 (2018). https://doi.org/10.1103/PhysRevD.97.075001. arXiv:1711.05743
99. P. Huang, Y.H. Ng, Di-Higgs production in SUSY models at the LHC. Eur. Phys. J. Plus **135**, 660 (2020). https://doi.org/10.1140/epjp/s13360-020-00677-1. arXiv:1910.13968
100. M. Mühlleitner, J. Schlenk, M. Spira, Top-Yukawa-induced corrections to Higgs pair production. JHEP **10**, 185 (2022). https://doi.org/10.1007/JHEP10(2022)185. arXiv:2207.02524
101. J. Davies, G. Mishima, K. Schönwald, M. Steinhauser, H. Zhang, Higgs boson contribution to the leading two-loop Yukawa corrections to gg $rightarrow$ HH. JHEP **08**, 259 (2022). https://doi.org/10.1007/JHEP08(2022)259. arXiv:2207.02587
102. J. Davies, K. Schönwald, M. Steinhauser, Towards $gg \to HH$ at next-to-next-to-leading order: light-fermionic three-loop corrections. arXiv:2307.04796
103. J. Davies, K. Schönwald, M. Steinhauser, H. Zhang, Next-to-leading order electroweak corrections to $gg \to HH$ and $gg \to gH$ in the large-$m_t$ limit. arXiv:2308.01355
104. H. Zhang, K. Schönwald, M. Steinhauser, J. Davies, Electroweak corrections to gg -> HH: Factorizable contributions. PoS **LL2024**, 014 (2024). https://doi.org/10.22323/1.467.0014. arXiv:2407.05787
105. H.-Y. Bi, L.-H. Huang, R.-J. Huang, Y.-Q. Ma, H.-M. Yu, Electroweak corrections to double Higgs production at the LHC. Phys. Rev. Lett. **132**, 231802 (2024). https://doi.org/10.1103/PhysRevLett.132.231802. arXiv:2311.16963
106. G. Heinrich, S. Jones, M. Kerner, T. Stone, A. Vestner, Electroweak corrections to Higgs boson pair production: the top-Yukawa and selfcoupling contributions. arXiv:2407.04653
107. D. Neacsu, Higgs Production at the LHC with colored scalars from B-meson decays models. Master's thesis, IST, University of Lisbon, 9 (2023)
108. ATLAS Collaboration, G. Aad et al., Constraints on the Higgs boson self-coupling from single- and double-Higgs production with the ATLAS detector using pp collisions at s = 13 TeV. Phys. Lett. B **843**, 137745 (2023). https://doi.org/10.1016/j.physletb.2023.137745. arXiv:2211.01216
109. J.R. Ellis, M.K. Gaillard, D.V. Nanopoulos, A phenomenological profile of the Higgs boson. Nucl. Phys. B **106**, 292 (1976). https://doi.org/10.1016/0550-3213(76)90382-5
110. M.A. Shifman, A.I. Vainshtein, M.B. Voloshin, V.I. Zakharov, Low-energy theorems for Higgs boson couplings to photons. Sov. J. Nucl. Phys. **30**, 711–716 (1979)
111. B.A. Kniehl, M. Spira, Low-energy theorems in Higgs physics. Z. Phys. C **69**, 77–88 (1995). https://doi.org/10.1007/s002880050007. arXiv:hep-ph/9505225
112. M.E. Peskin, T. Takeuchi, New constraint on a strongly interacting Higgs sector. Phys. Rev. Lett. **65**, 964–967 (1990). https://doi.org/10.1103/PhysRevLett.65.964
113. M.E. Peskin, T. Takeuchi, Estimation of oblique electroweak corrections. Phys. Rev. D **46**, 381–409 (1992). https://doi.org/10.1103/PhysRevD.46.381
114. W. Grimus, L. Lavoura, O.M. Ogreid, P. Osland, A precision constraint on multi-Higgs-doublet models. J. Phys. G Nucl. Part. Phys. **35**, 075001 (2008). https://doi.org/10.1088/0954-3899/35/7/075001
115. Particle Data Group Collaboration, R.L. Workman et al., Review of particle physics. PTEP **2022**, 083C01 (2022). https://doi.org/10.1093/ptep/ptac097
116. J. Alwall, C. Duhr, B. Fuks, O. Mattelaer, D.G. Öztürk, C.-H. Shen, Computing decay rates for new physics theories with FeynRules and MadGraph 5_aMC@NLO. Comput. Phys. Commun. **197**, 312–323 (2015). https://doi.org/10.1016/j.cpc.2015.08.031. arXiv:1402.1178
117. P. Gabriel, M. Mühlleitner, D. Neacsu, R. Santos, Hpair-scalars. (2023). https://gitlab.com/bdm-models/higgs-production/hpair-scalars. Accessed Dec 2023